

Envelope Expansion with Core Collapse II. Quasi-Spherical Self-Similar Solutions for an Isothermal Magnetofluid

Cong Yu^{1,5} * † and Yu-Qing Lou^{2,3,4}

¹National Astronomical Observatories/Yunnan Astronomical Observatory, Chinese Academy of Sciences, Kunming, 650011, China;

²Physics Department and Tsinghua Center for Astrophysics (THCA), Tsinghua University, Beijing, 100084, China;

³Department of Astronomy and Astrophysics, the University of Chicago, 5640 South Ellis Avenue, Chicago, IL 60637, USA;

⁴National Astronomical Observatories, Chinese Academy of Sciences, A20, Datun Road, Beijing 100012, China;

⁵Graduate School of the Chinese Academy of Sciences, Beijing, China.

Accepted 2005 ?? ?. Received 2005 ?? ??; in original form 2005 April ??

ABSTRACT

We investigate self-similar magnetohydrodynamic (MHD) processes in an isothermal self-gravitating fluid with a quasi-spherical symmetry and extend the envelope expansion with core collapse (EECC) solutions of Lou & Shen by incorporating a random magnetic field. Magnetized expansion-wave collapse solutions (MEWCS) can be readily constructed as a special case. This inside-out MHD collapse occurs at the magnetosonic speed and magnetized EECC solutions are obtained systematically. Stagnation surfaces of EECC solutions that separate core collapse and envelope expansion propagate at constant speeds either sub-magnetosonically or super-magnetosonically. These similarity MHD solutions show various behaviours, such as radial inflow or contraction, core collapse, oscillations and outflow or wind as well as shocks. For solutions to go across the magnetosonic line smoothly, we carefully analyze topological properties of magnetosonic critical points. Without crossing the magnetosonic critical line, continuous spectra of magnetized EECC and envelope contraction with core collapse (ECCC) solutions are readily obtained. Crossing the magnetosonic line twice analytically, there exists an infinite number of discrete magnetized EECC and ECCC solutions. One or more sub-magnetosonic stagnation surfaces associated with these discrete solutions travel outward at constant yet different speeds in a self-similar manner. In addition to the EECC shock solution which could change the central accretion rate, the magnetic field can also affect the core accretion rate. As the magnetic parameter λ increases, the core accretion rate appropriate for the MHD EWCS becomes larger. Under the frozen-in approximation, magnetic fields in the envelope expansion portion would scale as $B \propto r^{-1}$, while in the core collapse portion they would scale as $B \propto r^{-1/2}$. We discuss several astrophysical applications of EECC similarity solutions to the formation process of proto-planetary nebulae connecting the AGB phase and the planetary nebula, to supernova remnants, collapse of magnetized molecular cloud, to H II clouds surrounding massive OB stars and to a certain evolution phase of galaxy clusters.

Key words: magnetohydrodynamics – planetary nebulae: general – stars: AGB and post-AGB – stars: formation – stars: winds, outflows – waves

1 INTRODUCTION

The process of gravitational collapse is fundamental in various cosmological and astrophysical contexts, and is certainly one important phase for dynamical processes of star formation. Over decades, observational and theoretical studies have been combined together to outline a plausible scenario for such gravitational collapses in gaseous molecular clouds, taking account of geometrical factors

* A substantial part of this research publication was carried out at Physics Department and Tsinghua Center for Astrophysics (THCA) of Tsinghua University; this research publication serves as a partial fulfillment of PhD thesis requirement for C.Y.

† E-mail: yccit@yahoo.com.cn; louyq@mail.tsinghua.edu.cn and lou@oddjob.uchicago.edu

and other main physical considerations (e.g., Bodenheimer & Sweigart 1968). Self-similar solutions under the simplifying assumption of spherical symmetry have long been pursued in the past (Larson 1969a; Penston 1969a; Shu 1977; Hunter 1977, 1986; Whitworth & Summers 1985; Foster & Chevalier 1993). Independently, Penston (1969a,b) and Larson (1969a,b) started a simple analytical description of spherically symmetric isothermal collapse under the self-gravity that reproduced essential features of more detailed numerical simulations. In a seminal paper that introduced the current paradigm for an ‘inside-out collapse’ in low-mass star formation, Shu (1977) derived the so-called self-similar expansion wave collapse solution (EWCS). Subsequently, Hunter (1977) carried out a more comprehensive search and found an infinite number of discrete solutions in the ‘complete solution space’. Whitworth & Summers (1985) have considerably expanded these solutions into a two-parameter continuum by allowing for weak discontinuities across the sonic critical line.

For molecular clouds that are initially near a marginally stable equilibrium, the Larson-Penston (LP) solution provides a sensible approximation to the condition near the centre of the point mass (i.e., a protostar) formation epoch. Shu (1977) derived the EWCS that has a free-fall core collapse with a mass density profile of $\rho \propto r^{-3/2}$, a radial infall speed profile $u \propto r^{-1/2}$, a constant central mass accretion rate at $r \rightarrow 0^+$, and a static envelope of a singular isothermal sphere (SIS) with the collapsing front moving outward at the constant sound speed a , where r is the radial distance from the centre. This EWCS scenario of an inside-out collapse for star formation has been advocated by Shu, Adams & Lizano (1987) and compared with observations (Adams, Lada & Shu 1987; Zhou et al. 1993; Choi et al. 1995; Saito et al. 1999; Harvey et al. 2001). Foster & Chevalier (1993) studied the gravitational collapse of an isothermal sphere by hydrodynamical simulations and recovered the LP solution in the central region where a core forms and the self-similar solution of Shu (1977) when the ratio of initial outer cloud radius to core radius is $\gtrsim 20$.

Molecular gas clouds from which many stars come into being are structurally complex and highly filamentary in many places. The origin of such complex structures is not well understood at present. It may be partially produced by regular and random magnetic fields on different scales (e.g., Balick & Frank 2002). The formation of filaments and sheets may be necessary to the fragmentation of molecular clouds into clumps of order of the final stellar masses, although the relation between the initial cloud mass and the mass of the resulting stars remains unclear (e.g., Hartmann 1998). Due to the formation of filamentary structures in numerical simulations (Porter et al. 1994; Klessen & Burkert 2000; Ostriker et al. 2001) and the appearance of numerous filaments in observations (e.g., Falgarone et al. 2001), analyses on processes of filament formation and evolution have also been pursued in the literature (Kawachi & Hanawa 1998; Hennebelle 2003; Tilley & Pudritz 2003; Shadmehri 2005).

In view of the ubiquitous presence of magnetic fields in the interstellar medium and their nontrivial dynamic and diagnostic roles in astrophysical plasma systems, dynamical collapses of magnetized clouds have generated considerable interests. In some cases, magnetic fields may not be dynamically important, yet can offer valuable

diagnostic information through cyclotron or synchrotron emissions. Chiueh & Chou (1994) carried out an investigation of dynamical collapse in nonrotating magnetized gas clumps of grossly spherical shape. They focussed on the magnetic pressure effect with the magnetic tension effect being ignored. Effects of magnetic fields have also been extensively investigated in various contexts (Contopoulos et al. 1998; Krasnopolsky & Königl 2002; Hennebelle 2003; Tilley & Pudritz 2003; Shadmehri 2005). In terms of theoretical formulation and astrophysical applications, we note that magnetic field can make a tenuous collisionless gas to behave more fluid like as evidenced by fusion plasma experiments and solar wind observations. As a result, we could study dilute magnetized plasmas on large scales using the MHD description.

Thermal radio emissions from planetary nebulae have been observed (Kwok 1982, 1985, 1993) and might perhaps indicate the presence of magnetic fields. By extensive observations of various morphologies, it is most likely that magnetic field should influence the shapes and shaping of PNe (e.g. Balick & Frank 2002). Although not a PN, the remnant morphology of a triple ring system of the supernova SN 1987A may also hint at important roles of magnetic field as modelled through numerical simulations (Tanaka & Washimi 2002). Within the collapsed core of a PN, magnetic dynamo processes may also operate for some time to generate and sustain a strong magnetic field (e.g., $\sim 10^4 - 10^9$ G) associated with a proto-white dwarf (Blackman et al. 2001).

The role of magnetic field in our model analysis is characterized by one important parameter λ as defined by equation (16). Different systems of astrophysical objects involve various values of λ . The estimated λ parameter for the Crab Nebula is of the order of a magnitude $\sim 10^5$. For a galaxy cluster, the estimated λ is approximately 0.2. For star forming regions, the estimated λ is typically 0.01. For planetary nebulae, the typical λ is approximately ~ 0.003 .

In addition to collapses and flows with an isothermal equation of state, gravitational collapses with polytropic or logotropic equations of state have also been investigated by several authors (Cheng 1978; Goldreich & Weber 1980; Bouquet et al. 1985; Suto & Silk 1988; McLaughlin & Pudritz 1997; Kawachi & Hanawa 1998; Scalo et al. 1998; Maeda et al. 2002; Harada et al. 2003; Shadmehri 2005). With a polytropic equation of state, the gravitational bound system have different temperatures at different radii. It is also possible to include effects of radiative losses in the energy equation (e.g., Boily & Lynden-Bell 1995; Murakami, Nishihara & Hanawa 2004). Stability of self-similar gravitational collapses was also considered by several authors (Ori & Piran 1988; Hanawa 1997; Hanawa & Matsumoto 1999, 2000; Lai & Goldreich 2000; Lai 2000). Lai & Goldreich (2000) studied the growth of nonspherical perturbations in the collapse of a self-gravitating spherical gas cloud. They found that nonspherical perturbations damp in the subsonic region and grow in the supersonic region. They mentioned potential applications to core collapse of supernova explosions (Cheng 1978; Goldreich & Weber 1980; Yahil 1983), where asymmetric density perturbations may lead to asymmetric shock propagation and breakout, giving rise to asymmetry in the explosion and a kick to a new-borne neutron star. Global stability

analysis with a polytropic equation of state was also carried out by Lai (2000). Slow rotation effects on gravitational collapses has been considered by Terebey, Shu & Cassen (1984). As an important extension of Shu (1977), the general relativistic analysis of collapse or accretion onto a black hole has been recently conducted by Cai & Shu (2005).

Recently, Lou & Shen (2004) examined self-similar spherical isothermal collapses and derived new solutions in the semi-complete solution space; this is in reference to the ‘complete solution space’ of Hunter (1977). The gas flow at large r , together with the two distinct asymptotic solution behaviours near the origin, lead to an infinite number of discrete self-similar solutions that are analytically smooth across the sonic critical line. Those solutions characterized by envelope expansion with core collapse (EECC) are of particular interest. In various contexts of astrophysical systems, it would be natural and important to include effects of magnetic fields in a collapsing cloud. Our main motivation here is to study this generalized class of EECC solution in the presence of a random magnetic field. Meanwhile, we broaden and enrich all the known similarity solution structures in the most general manner.

In the presence of magnetic field, the exact spherical symmetry for a magnetized flow no longer exists in the rigorous sense. Nevertheless, morphological observations of supernova remnants, such as the Crab Nebula, show that gross quasi-elliptical structures do exist on large scales. With these empirical considerations in mind, we develop an MHD formalism for a quasi-spherical symmetry for large-scale magnetized flows. The close analogy between the mass conservation equation and the magnetic induction equation gives rise to a special relation connecting the gas mass density, the magnetic field component transverse to the radial flow direction and the radius r . With this relation, magnetic field can be readily incorporated into the EECC framework (Lou & Shen 2004). This paper is to investigate the magnetic field effects on the EECC solutions under the approximation of a quasi-spherical symmetry.

Besides these shock-free globally smooth solutions, Tsai & Hsu (1995) constructed a self-similar shock solution describing a situation in which a central thermal or kinetic energy release initiates an outgoing shock during a proto-stellar collapse of a low-mass star. Such a shock solution, matched with a static SIS envelope, can have a central free-fall collapse, yet with a central mass accretion rate lower than that predicted by the EWCS. Tsai & Hsu (1995) also constructed a shock expansion solution with a finite core density matched with a static SIS envelope; this solution has been recently generalized and subsumed into a family of ‘champagne flow’ shock solutions by (Shu et al. 2002) to model expansions of H II regions surrounding massive OB stars after the passage of an initial ionization front. To be more general, Shen & Lou (2004) studied EECC shock solutions allowing outflows or inflows far away from the central region. In terms of modelling proto-stellar systems, this flexibility can accommodate a variety of real possibilities. Most recently, Bian & Lou (2005) explored the parameter space more systematically to construct various isothermal shock solutions, including for example, twin shocks, and so forth.

This paper is structured as follows. The basic MHD equations and the self-similar transformation are presented in § 2. In § 3, we provide a comprehensive analysis of the

resulting nonlinear MHD ODEs. In § 4, we solve the nonlinear MHD ODEs numerically with the help of necessary analytical analysis given in § 3. In § 5, we give the physical interpretations of our results.

2 PHYSICAL ASSUMPTIONS AND BASIC MODEL FORMULATION

We adopt the isothermal approximation for the gas under consideration. By the quasi-spherical symmetry of a magnetized flow system, the basic MHD equations in spherical polar coordinates (r, θ, ϕ) are:

$$\frac{\partial \rho}{\partial t} + \frac{1}{r^2} \frac{\partial(r^2 \rho u)}{\partial r} = 0, \quad (1)$$

$$\frac{\partial M}{\partial r} = 4\pi \rho r^2 \quad (2)$$

for the mass conservation, where u is the bulk radial flow speed, ρ is the gas mass density and $M(r, t)$ is the enclosed mass within r at time t . By the definition of $M(r, t)$, we have the equivalent of equation (1), namely

$$\frac{\partial M}{\partial t} + u \frac{\partial M}{\partial r} = 0. \quad (3)$$

The radial momentum equation is simply

$$\frac{\partial u}{\partial t} + u \frac{\partial u}{\partial r} = -\frac{a^2}{\rho} \frac{\partial \rho}{\partial r} - \frac{GM}{r^2} - \frac{1}{8\pi \rho} \frac{\partial}{\partial r} \langle B_{\perp}^2 \rangle - \frac{\langle B_{\perp}^2 \rangle}{4\pi \rho r} \quad (4)$$

where $-\partial\Phi/\partial r \equiv -GM(r, t)/r^2$ with $\Phi(r, t)$ being the gravitational potential and B_{\perp} is the magnitude of the magnetic field transverse to the radial direction. The Poisson equation relating the gas mass density ρ and the gravitational potential Φ is automatically satisfied. Here in equation (4), we keep the magnetic tension force term that was ignored in equation (3) of Chiueh & Chou (1994).

The MHD energy conservation takes the form of

$$\begin{aligned} \frac{\partial}{\partial t} \left\{ \frac{\rho u^2}{2} + a^2 \rho \left[\ln \left(\frac{\rho}{\rho_c} \right) - 1 \right] - \frac{1}{8\pi G} \left(\frac{\partial \Phi}{\partial r} \right)^2 + \frac{\mathbf{B}^2}{8\pi} \right\} \\ + \frac{1}{r^2} \frac{\partial}{\partial r} \left\{ r^2 u \rho \left[\frac{u^2}{2} + a^2 \ln \left(\frac{\rho}{\rho_c} \right) \right] \right\} \\ + \frac{1}{r^2} \frac{\partial}{\partial r} (r^2 u \rho \Phi) + \frac{1}{r^2} \frac{\partial}{\partial r} \left(\frac{r^2 \Phi}{4\pi G} \frac{\partial^2 \Phi}{\partial r \partial t} \right) \\ + \nabla \cdot \left[\frac{\mathbf{B}}{4\pi} \times (\mathbf{u} \times \mathbf{B}) \right] = 0, \quad (5) \end{aligned}$$

which generalizes equation (4) of Lou & Shen (2004) by including the magnetic field \mathbf{B} ; the magnetic energy density and the Poynting flux density can be readily identified, respectively. We derive this MHD energy conservation equation when all magnetic field components are included.

To reach the above MHD energy conservation equation, we have taken the electrical conductivity to be infinite, such that the magnetic induction equation takes the form of

$$\frac{\partial \mathbf{B}}{\partial t} = \nabla \times (\mathbf{u} \times \mathbf{B}). \quad (6)$$

The three component forms of this magnetic induction equation are

$$\frac{\partial B_r}{\partial t} = \frac{1}{r \sin \theta} \frac{\partial}{\partial \theta} \left[\sin \theta (u_r B_\theta - u_\theta B_r) \right] - \frac{1}{r \sin \theta} \frac{\partial}{\partial \phi} (u_\phi B_r - u_r B_\phi), \quad (7)$$

$$\frac{\partial B_\theta}{\partial t} = \frac{1}{r \sin \theta} \frac{\partial}{\partial \phi} (u_\theta B_\phi - u_\phi B_\theta) - \frac{1}{r} \frac{\partial}{\partial r} \left[r (u_r B_\theta - u_\theta B_r) \right], \quad (8)$$

$$\frac{\partial B_\phi}{\partial t} = \frac{1}{r} \frac{\partial}{\partial r} \left[r (u_\phi B_r - u_r B_\phi) \right] - \frac{1}{r} \frac{\partial}{\partial \theta} (u_\theta B_\phi - u_\phi B_\theta), \quad (9)$$

where $u_r \equiv u$ in our formalism. We just consider radial bulk flow $u_r \neq 0$ by setting $u_\theta = u_\phi = 0$, equation (7) then becomes

$$\frac{\partial B_r}{\partial t} = u_r (\nabla_\perp \cdot \mathbf{B}_\perp) + (\mathbf{B}_\perp \cdot \nabla) u_r. \quad (10)$$

Using the divergence-free condition of magnetic field $\nabla \cdot \mathbf{B} = 0$, equation (10) becomes

$$\frac{1}{2} \frac{D}{Dt} [(r^2 B_r)^2] = r^4 B_r (\mathbf{B}_\perp \cdot \nabla) u_r, \quad (11)$$

where $D/Dt \equiv \partial/\partial t + u_r \partial/\partial r$. The θ - and ϕ -components of the magnetic induction equations (8) and (9), under the simplifying approximation of $u_\theta = 0$ and $u_\phi = 0$, become

$$\frac{D}{Dt} \ln \left(\frac{B_\theta}{r} \right) = -\frac{1}{r^2} \frac{\partial}{\partial r} (r^2 u_r), \quad (12)$$

$$\frac{D}{Dt} \ln \left(\frac{B_\phi}{r} \right) = -\frac{1}{r^2} \frac{\partial}{\partial r} (r^2 u_r). \quad (13)$$

The continuity equation of mass conservation takes a similar form in parallel, namely

$$\frac{D}{Dt} \ln \rho = -\frac{1}{r^2} \frac{\partial}{\partial r} (r^2 u_r). \quad (14)$$

From the above three equations (12)–(14), we obtain

$$\frac{B_\theta}{\rho r} = \text{const}, \quad \frac{B_\phi}{\rho r} = \text{const}, \quad \frac{B_\perp}{\rho r} = \text{const}, \quad (15)$$

where $B_\perp = (B_\theta^2 + B_\phi^2)^{1/2}$ is the magnitude of the magnetic field component transverse to the radial component.

Based on the last of integrals (15), we introduce a simple relation

$$B_\perp^2 = 16\pi^2 \lambda G \rho^2 r^2 \quad (16)$$

with the magnetic parameter λ being a proportional constant. In comparison with the work of Chiueh & Chou (1994), it is apparent that

$$\lambda = \frac{\beta(x)}{\alpha^2 x^2},$$

where $\beta(x)$ is a dimensionless function introduced by Chiueh & Chou (1994) and α is our reduced density. Note that the ratio of the Alfvén speed v_A to the isothermal sound speed a is given by

$$\frac{v_A}{a} = \left(\frac{\beta}{\alpha} \right)^{1/2} \quad \text{and} \quad v_A \equiv \frac{B_\perp}{(4\pi\rho)^{1/2}}.$$

Similarity solutions with x ranging from $x \rightarrow +\infty$ to $x \rightarrow 0^+$ are referred to as the semi-complete solutions (Shu 1977; Whitworth & Summers 1985; Lou & Shen 2004; Shen & Lou 2004). Similarity solutions with x ranging from $x \rightarrow -\infty$ to $x \rightarrow +\infty$ are referred to as complete solutions (Hunter 1977, 1986). The perspectives of complete (Hunter 1977, 1986) and semi-complete (Shu 1977; Whitworth & Summers 1985; Lou & Shen 2004) similarity solutions are both valid with appropriate physical interpretations and with the proper specification of an initial moment. For the invariance under the time reversal transformation of self-gravitational magnetofluid equations (1)–(4), namely, $t \rightarrow -t$, $\rho \rightarrow \rho$, $u \rightarrow -u$, the semi-complete and complete similarity solutions are in fact closely related to each other. Complete Hunter type solutions can be decomposed into two branches of similarity solutions in the semi-complete space (Lou & Shen 2004). Furthermore, the time reversal transformation can also lead to different interpretations and application of self-similar solutions. In this paper, we focus on the semi-complete solutions. For ideal MHD equations with an infinite electric conductivity, the magnetic induction equation (6) is invariant under $t \rightarrow -t$ and $\vec{v} \rightarrow -\vec{v}$ transformation. In fact, the corresponding transformation of either $\vec{B} \rightarrow \vec{B}$ or $\vec{B} \rightarrow -\vec{B}$ is allowed. If we take the magnetic diffusion term into account, these invariant properties are no longer valid.

We now introduce the self-similar transformation:

$$\rho(r, t) = \frac{\alpha(x)}{4\pi G t^2},$$

$$M(r, t) = \frac{a^3 t}{G} m(x),$$

$$u(r, t) = a v(x), \quad (17)$$

$$\Phi(r, t) = a^2 \phi(x),$$

$$B_\perp = \frac{a}{\sqrt{Gt}} b(x),$$

and immediately get

$$b(x) = \sqrt{\lambda} \alpha x,$$

where $x \equiv r/(at)$ is the independent self-similar variable; the dimensionless $\alpha(x)$, $m(x)$, $v(x)$, $\phi(x)$ and $b(x)$ are the reduced dependent variables for the gas mass density, the enclosed mass, the radial flow speed, the gravitational potential and the transverse magnetic field, respectively. They are all functions of x only. Note that $b(x)$ is related to $\beta(x)$ of Chiueh & Chou (1994) by $b^2 \equiv \beta$. After a direct substitution of the above transformations into the nonlinear MHD partial differential equations, we obtain the following nonlinear ordinary differential equations (ODEs).

It follows that equations (2) and (3) reduce to

$$m' = x^2 \alpha, \quad (18)$$

$$(v-x)m' + m = 0, \quad (19)$$

where the prime denotes the derivative with respect to x . Combining these two equations, we immediately obtain the following two equations

$$m = (x-v)x^2 \alpha, \quad (20)$$

$$\frac{d}{dx} [x^2 \alpha (x-v)] = x^2 \alpha. \quad (21)$$

By equation (20), the physical condition of a positive mass $m(x) > 0$ is transformed into the condition of $x - v > 0$. Therefore, solutions of $v(x)$ must lie to the upper-right of the straight line $x - v = 0$ in the plane $-v(x)$ versus x .

The continuity equation of mass conservation becomes

$$v' + (v - x)\frac{\alpha'}{\alpha} = \frac{2}{x}(x - v) \quad (22)$$

and the radial momentum equation becomes

$$(v - x)v' + (1 + \lambda\alpha x^2)\frac{\alpha'}{\alpha} = -\alpha(x - v) - 2\lambda x\alpha. \quad (23)$$

Rearranging these two equations above, we arrive at

$$\begin{aligned} & \left[(x - v)^2 - (1 + \lambda\alpha x^2) \right] v' \\ & = (x - v) \left[\alpha(x - v) - \frac{2}{x} \right] \end{aligned} \quad (24)$$

and

$$\begin{aligned} & \left[(x - v)^2 - (1 + \lambda\alpha x^2) \right] \frac{\alpha'}{\alpha} \\ & = (x - v) \left[\alpha - \frac{2}{x}(x - v) \right] + 2\lambda x\alpha. \end{aligned} \quad (25)$$

Note that by setting $\lambda = 0$ for the absence of magnetic field, we readily recover the formulation of Lou & Shen (2004). For smooth and regular solutions crossing the magnetosonic line, the critical conditions are

$$(x - v) \left[\alpha(x - v) - \frac{2}{x} \right] = 0, \quad (26)$$

$$(x - v)^2 - (1 + \lambda\alpha x^2) = 0, \quad (27)$$

$$(x - v) \left[\alpha - \frac{2}{x}(x - v) \right] + 2\lambda x\alpha = 0 \quad (28)$$

in order to determine finite first derivatives v' and α' , respectively. In fact, only two of the above three requirements are independent. For $x - v \neq 0$, the above three equations are equivalent to the following three equations

$$x - v = \frac{2}{\alpha x}, \quad (29)$$

$$\alpha^2 x^2 + \lambda\alpha^3 x^4 = 4, \quad (30)$$

$$(x - v) + 2\lambda x = (x - v)^3. \quad (31)$$

For $\lambda = 0$, equation (31) becomes $(x - v) = \pm 1$ and equation (30) reduces to $\alpha = 2/x$. Given the positiveness of $x - v > 0$, we then come to the familiar critical condition $x - v = 1$ (Lou & Shen 2004). Equation (27) for $(x - v)^2 - (1 + \lambda\alpha x^2) = 0$ is equivalent to the condition $(x - v)^2 = (a^2 + v_A^2)/a^2$ in dimensional form, directly related to the magnetosonic condition.

3 ANALYSIS OF NONLINEAR ODES

3.1 Special Analytical Solutions

With $\phi' = mx^{-2}$, an exact global analytical solution of nonlinear ODEs (24) and (25) appears in the form of

$$v = 0, \quad \alpha = \frac{2}{x^2}, \quad m = 2x, \quad \frac{d\phi}{dx} = \frac{2}{x}, \quad b = \frac{2\lambda^{1/2}}{x}, \quad (32)$$

which describes a magnetostatic equilibrium for a quasi-spherical system (Ebert 1955; Bonnor 1956; Chandrasekhar 1957; Shu 1977). In physical dimensions, we simply have

$$\rho = \frac{a^2}{2\pi Gr^2}, \quad M = \frac{2a^2 r}{G}, \quad B_{\perp}^2 = \frac{4\lambda a^4}{Gr^2}.$$

In this solution, the magnetic pressure gradient force density and the magnetic tension force density cancel each other (i.e., a nearly force-free magnetic field), that is, their combined effects on the entire system are absent. To be more specific but in dimensionless form, the sum of the magnetic pressure gradient and tension force densities is simply

$$-\lambda(\alpha' x^2 + 2\alpha x) = 0.$$

Another exact global analytical similarity solution of nonlinear ODEs (24) and (25) is

$$\begin{aligned} v &= \frac{2}{3}x, \quad \alpha = \frac{2}{(3 + 18\lambda)}, \quad m = \frac{2x^3}{3(3 + 18\lambda)}, \\ \frac{d\phi}{dx} &= \frac{2x}{3(3 + 18\lambda)}, \quad b = \frac{2\lambda^{1/2}x}{(3 + 18\lambda)}. \end{aligned} \quad (33)$$

In physical dimensions, we simply have

$$\rho = \frac{1}{2(3 + 18\lambda)\pi Gt^2}, \quad M = \frac{2r^3}{3(3 + 18\lambda)Gt^2},$$

$$B_{\perp}^2 = \frac{4\lambda r^2}{G(3 + 18\lambda)^2 t^4}.$$

Within a finite radius r , the transverse magnetic field strength $|B_{\perp}|$ scales as t^{-2} . This solution passes the magnetosonic critical line at $x = 3(1 + 6\lambda)^{1/2}$ as would be evident in our later discussion about the MHD generalization of the Larson-Penston-type solutions. In the absence of magnetic field with $\lambda = 0$, this solution passes the sonic critical line at $x = 3$ (Whitworth & Summers 1985). Such solution corresponds to a nonrelativistic Einstein-de Sitter expansion with magnetic field. Here, the ‘cosmic mass density’ is $\rho = 1/[(6 + 36\lambda)\pi Gt^2]$ and the relevant ‘Hubble constant’ is $H = 2/[3t(1 + 6\lambda)^{1/2}]$ that decreases with time t .

Another exact global solution is the singular solution

$$x - v = \frac{2}{\alpha x} \quad \text{and} \quad (x - v)^2 - (1 + \lambda\alpha x^2) = 0, \quad (34)$$

which actually specifies the magnetosonic critical line. This set of equations for the magnetosonic critical line shall be discussed in more details presently.

The second condition of equation (34) is equivalent to

$$a(x - v) = (v_A^2 + a^2)^{1/2};$$

the right-hand side is the magnetosonic speed and the left-hand side is the wave front speed relative the local flow speed. When the Doppler-shifted flow speed coincides with the local magnetosonic speed, the singularity would arise. The situation appears to be similar to the discussion of the ‘nozzle condition’ in the steady solar wind (Parker 1963), or to the discussion of the critical accretion rate in a steady spherical accretion (Bondi 1952).

3.2 Results for Crossing the Magnetosonic Critical Line

The coupled nonlinear MHD equations are singular along the magnetosonic critical line. Because of this, we cannot directly obtain similarity solutions that go across the magnetosonic critical line smoothly by a simple-minded numerical integration backward from $x \rightarrow +\infty$. To obtain solutions satisfying magnetosonic critical conditions (29) – (31), we need to first derive non-trivial first derivatives of v and α by applying the L'Hôpital rule along the magnetosonic critical line. Higher-order derivatives of v and α across the magnetosonic critical line can also be determined accordingly (Hunter 1986; Whitworth & Summers 1985). It is straightforward to derive a quadratic equation for $z \equiv v'$, namely

$$2 \left[(v-x) - \frac{x\lambda}{(v-x)^2} \right] z^2 + 2(x-v)z - \frac{2v}{x^2} = 0 \quad (35)$$

(see Appendix B for a detailed derivation).

Solving this quadratic equation, together with equation (29), (31) and (22), we obtain the first derivative v' along the magnetosonic critical line. Once the first derivative v' is known, we immediately obtain the first derivative α' using equations (22) or (23). By this procedure, the problem of crossing the magnetosonic critical line smoothly and analytically has been completely solved by means of an effective numerical scheme. For quadratic equation (35), analytical expansions could be found once the coefficients of this equation can be given explicitly. We have solved the magnetosonic critical line equation as described later in this section, that is, we know the value of v for a given value of x along the magnetosonic critical line. Thus analytical eigensolutions of equation (35) can be given, as all the coefficients of the equation (35) can be expressed in terms of x . However, such explicit eigensolutions of equation (35) would be very complex and it would be more convenient to derive the two eigensolutions numerically.

In comparison with equations (16) – (18) of Chiueh & Chou (1994), we find that their results about the magnetosonic critical point is a very special case of ours. By setting $v = 0$, we get similar results as those of Chiueh & Chou (1994). Their equations (16) – (18) are results about the zero point $x_c = (1 + 2\lambda)^{1/2}$. Expressing our results related to the zero point in terms of their similar notations, we have

$$\lambda = \frac{x_c^2 - 1}{2}, \quad \alpha_c = \frac{2}{x_c^2}, \quad \beta_c = b_c^2 = \frac{2(x_c^2 - 1)}{x_c^2},$$

$$v_c = 0, \quad v'_{c1} = \frac{2x_c^2}{3x_c^2 - 1}, \quad v'_{c2} = 0, \quad (36)$$

$$\alpha'_{c1} = -\frac{4(2x_c^2 - 1)}{x_c^3(3x_c^2 - 1)}, \quad \alpha'_{c2} = -\frac{4}{x_c^3}, \quad (37)$$

$$\beta'_{c1} = 2\lambda\alpha_c\alpha'_{c1}x_c^2 + 2\lambda\alpha_c^2x_c = -\frac{8\lambda(x_c^2 - 1)}{x_c^3(3x_c^2 - 1)}, \quad (38)$$

$$\beta'_{c2} = 2\lambda\alpha_c\alpha'_{c2}x_c^2 + 2\lambda\alpha_c^2x_c = -\frac{8\lambda}{x_c^3}. \quad (39)$$

Note that $\lambda \geq 0$ and thus $x_c \geq 1$ (Chiueh & Chou 1994). The derivative of $b = \lambda^{1/2}\alpha x$ can be calculated once results of α are known. The key difference lies in the fact that our momentum equation contains the magnetic tension force

term that was ignored in their formulation. These results are crucial for constructing MHD expansion-wave collapse solutions (MEWCSs) (Shu 1977; Chiueh & Chou 1994).¹

By equation (35), there are two types of eigensolutions for $z \equiv v'$ at each point along the magnetosonic critical line. When the two roots of equation (35) are of opposite signs, type 1 and type 2 eigensolutions are referred to those with negative and positive roots of the equation (35), respectively. When the two roots of equation (35) are of the same sign, type 1 and 2 eigensolutions are those with smaller and larger absolute values respectively, following the nomenclature of Shu (1977) and Lou & Shen (2004). In Lou & Shen (2004), type 1 corresponds to $dv/dx = 1 - 1/x_*$ and type 2 corresponds to $dv/dx = 1/x_*$. In the open range of $0 < x < 2$, type 1 and type 2 are exactly defined as such. When $x > 2$ (relevant to the LP-type solution), dv/dx of type 1 has a larger absolute value, while dv/dx of type 2 has a smaller absolute value, that is, their magnitudes reverse for nodal points. In our current definition, no magnitude reversal would happen. When the point is a nodal point, type 1 and type 2 solutions remain always the smaller and larger ones respectively for the absolute value of dv/dx . To summarize, our definition is not defined by the explicit expressions of dv/dx (e.g., $1 - 1/x_*$ and $1/x_*$), but by their magnitudes and signs. It is easier to keep in mind their relevant physical properties.

As a necessary consistent check, we note that when $\lambda = 0$ and $x - v = 1$, the familiar results of Shu (1977) are readily recovered, namely

$$-2z^2 + 2z - \frac{2(x-1)}{x^2} = 0. \quad (40)$$

The two eigensolutions of this quadratic equation are simply

$$z_1 = \frac{1}{x_*}, \quad z_2 = 1 - \frac{1}{x_*}$$

[see the Appendix of Shu (1977)].

Expanding equation (31) and regrouping terms, we obtain the following cubic equation in terms of $v(x)$

$$v^3 + a_2v^2 + a_1v + a_0 = 0 \quad (41)$$

describing the magnetosonic critical line, where the three coefficients are $a_2 = -3x$, $a_1 = 3x^2 - 1$ and $a_0 = 2\lambda x + x - x^3$. This equation can be solved for v in terms of x . Let z_1, z_2, z_3 be the three roots of cubic equation (41) in terms of x . By the properties of a cubic equation, it follows that

$$z_1 + z_2 + z_3 = -a_2, \quad (42)$$

$$z_1z_2 + z_2z_3 + z_3z_1 = a_1, \quad (43)$$

$$z_1z_2z_3 = -a_0. \quad (44)$$

Following the standard procedure of solving a cubic algebraic equation, we then introduce two dimensionless parameter q and r such that

$$q = \frac{a_1}{3} - \frac{a_2^2}{9}, \quad (45)$$

$$r = \frac{(a_1a_2 - 3a_0)}{6} - \frac{a_2^3}{27}. \quad (46)$$

¹ We note in passing that equations (1)–(3) and (8)–(10) of Chiueh & Chou (1994) are somehow inconsistent. The magnetosonic critical condition in their analysis is correct.

It then follows that

$$q^3 + r^2 = \frac{1}{3} \left(\frac{a_1}{6} \right)^2 (4a_1 - a_2^2) + a_0 \left(\frac{a_2}{3} \right)^3 + \frac{a_0^2}{4} - \frac{a_0 a_1 a_2}{6}. \quad (47)$$

For $q^3 + r^2 > 0$, the cubic equation possesses one real root for v and a pair of complex conjugate roots for v . For $q^3 + r^2 = 0$, all three roots of v are real and at least two of them are equal. For $q^3 + r^2 < 0$, all three roots of v are real. In cubic equation (41), v is the unknown for a given x . In solving for v , we express the three roots z_i as

$$z_1 = (s_1 + s_2) - a_2/3, \quad (48)$$

$$z_{2,3} = -\frac{(s_1 + s_2)}{2} - \frac{a_2}{3} \pm \frac{i\sqrt{3}}{2}(s_1 - s_2), \quad (49)$$

where the two parameters s_1 and s_2 are defined by

$$s_{1,2} \equiv [r \pm (q^3 + r^2)^{1/2}]^{1/3}.$$

Specific to the current problem, we simply have

$$q = -1/3, \quad (50)$$

$$r = -x\lambda \quad (51)$$

and

$$q^3 + r^2 = x^2\lambda^2 - 1/27, \quad (52)$$

when

$$x \geq 1/(3\sqrt{3}\lambda); \quad (53)$$

the only real root is the one given by equation (48). Given an explicit expression of this root, we can analyze the nodal or saddle properties along the magnetosonic critical line (e.g., Jordan & Smith 1977). For $x \leq (3\sqrt{3}\lambda)^{-1}$, we need to identify the suitable root lying in the required parameter regime to satisfy $x - v > 0$. This is somewhat more involved than the case of $x \geq (3\sqrt{3}\lambda)^{-1}$.

For the case of $x \leq (3\sqrt{3}\lambda)^{-1}$, we adopt an alternative solution procedure by introducing a transitional variable

$$\theta \equiv \arccos \left(\frac{-r}{\sqrt{-q^3}} \right) = \arccos(3\sqrt{3}x\lambda), \quad (54)$$

where θ lies in the range $0 \leq \theta \leq \pi/2$. The three roots of the cubic equation can be expressed more compactly and neatly in terms of this θ parameter (Press et al. 1986), namely

$$z_1 = -2\sqrt{-q} \cos \left(\frac{\theta}{3} \right) - \frac{a_2}{3} = -\frac{2\sqrt{3}}{3} \cos \left(\frac{\theta}{3} \right) + \frac{x}{3}, \quad (55)$$

$$z_{2,3} = -2\sqrt{-q} \cos \left(\frac{\theta \pm 2\pi}{3} \right) - \frac{a_2}{3} = -\frac{2\sqrt{3}}{3} \cos \left(\frac{\theta \pm 2\pi}{3} \right) + \frac{x}{3}. \quad (56)$$

Since $\theta/3$ falls in the range of $0 \leq \theta \leq \pi/6$, it follows that $\cos(\theta/3)$ is positive while $\cos(\theta/3 + 2\pi/3)$ and $\cos(\theta/3 - 2\pi/3)$ are both negative. Therefore, z_2 and z_3 must be positive,

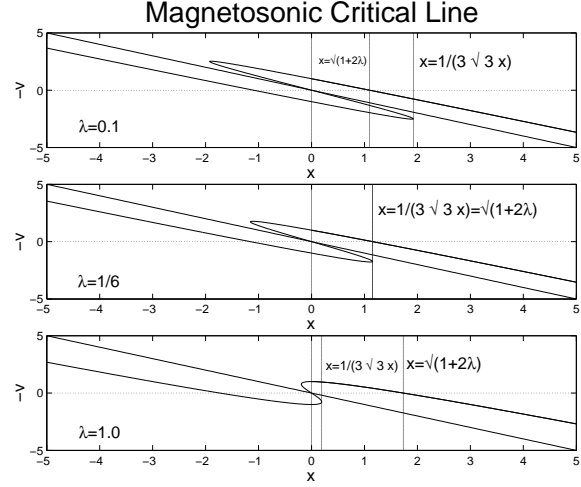


Figure 1. The magnetosonic critical lines for $\lambda = 0.1, 1/6, 1.0$ in upper, middle, lower panels, respectively; the vertical coordinate is the negative reduced radial speed $-v \equiv -u/a$ and the horizontal coordinate is the independent similarity variable $x \equiv r/(at)$. In the upper panel for $\lambda = 0.1$, the zero point is to the left of the turning point. In the middle panel for $\lambda = 1/6$, the zero point and the turning are at the same location. In the lower panel for $\lambda = 1$, the zero point is to the right of the turning point. This diagram is consistent with our analytical analysis. The diagonal straight line from the upper-left to the bottom-right in each panel is $x - v = 0$.

while z_1 may be either positive or negative. The zero point (i.e., $-v = 0$) of the magnetosonic critical line is at

$$x = (1 + 2\lambda)^{1/2}. \quad (57)$$

The other special location is

$$x = 1/(3\sqrt{3}\lambda) \quad (58)$$

that separates $-v$ regimes for one root (for larger $|x|$) and three real roots (for smaller $|x|$). By equating these two special locations, we have

$$\lambda_* = 1/6. \quad (59)$$

We refer to the point with abscissa $x = 1/(3\sqrt{3}\lambda)$ in the fourth quadrant as the turning point along the magnetosonic critical line. In Figure 1, we see that for $\lambda = 1/6$, the zero point and the turning point of the curve in the fourth quadrant have the same abscissa x as expected. For $\lambda < 1/6$, the abscissa of the zero point is smaller than that of the turning point in the fourth quadrant, while for $\lambda > 1/6$, the abscissa of the zero point is larger than that of the turning point of the curve in the fourth quadrant. From the three panels in Fig. 1, we conclude that the magnetosonic critical lines are connected smoothly by the two solutions (55) and (48) at $x = (3\sqrt{3}\lambda)^{-1}$. A quick summary for the magnetosonic critical line in terms of $-v$ is as follows: when $x \leq (3\sqrt{3}\lambda)^{-1}$, $z_1 = -(2/\sqrt{3}) \cos(\theta/3) + x/3$; when $x \geq (3\sqrt{3}\lambda)^{-1}$, $z_1 = s_1 + s_2 + x/3$. Once the magnetosonic critical line in terms of $v(x)$ is obtained, the corresponding magnetosonic critical line for $\alpha(x)$ can be readily determined by equation (29). In Figure 2, we explore variations of the magnetosonic critical lines for different values of λ . By the time reversal symmetry of the magnetosonic critical line, we

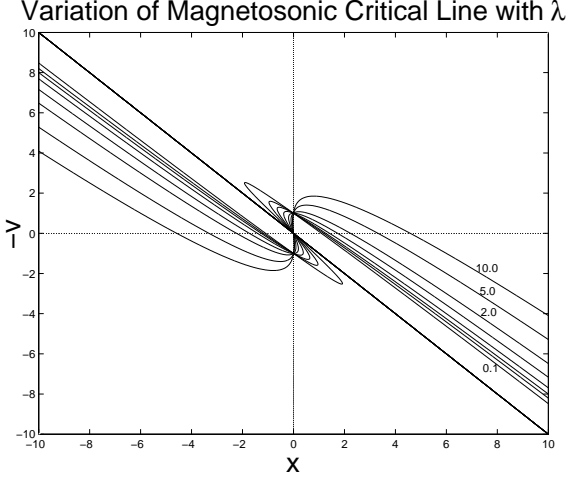


Figure 2. We choose $\lambda = 0.1, 0.2, 0.3, 0.5, 1.0, 2.0, 5.0, 10.0$ (from the lower part to the top part in order in the first and fourth quadrants); the vertical coordinate is the negative reduced radial speed $-v \equiv -u/a$ and the horizontal coordinate is the independent self-similarity variable $x \equiv r/(at)$. It is clear in this figure that in the first and fourth quadrants, all the magnetosonic critical lines lie above the straight line $-v = \sqrt{3}/3 - x$. This information is essential for our analysis of the nodal and saddle points in Appendix B. The diagonal straight line from the upper-left to the bottom-right is $x - v = 0$.

plot them in the entire plane. Our focus is mainly on the first and fourth quadrants.

3.3 Asymptotic Solutions of Nonlinear ODEs

Solution behaviours of nonlinear ODEs (24) and (25) at infinity ($x \rightarrow +\infty$) show effects of magnetic field (i.e., $\lambda \neq 0$) in the higher order terms, as seen clearly from the following expressions of asymptotic expansions

$$v = V + \frac{2-A}{x} + \frac{V}{x^2} + \frac{(A/6-1)(A-2) + 2V^2/3 + A(2-A)\lambda/3}{x^3} + \dots, \quad (60)$$

$$\alpha = \frac{A}{x^2} + \frac{A(2-A)}{2x^4} + \frac{A(4-A)V}{3x^5} + \frac{A(A-3)(A/2-1) - (A-6)AV^2/4 + (2-A)A^2\lambda/4}{x^6} + \dots, \quad (61)$$

$$\beta = \lambda\alpha^2 x^2 = \frac{A^2\lambda}{x^2} + \frac{A^2(2-A)\lambda}{x^4} + \frac{A^2(2-A)^2\lambda}{4x^6} + \dots, \quad (62)$$

where V , A and λ are three integration constants referred to as the speed, density and magnetic field parameters, respectively. The magnetic field parameter λ comes into play fairly late in the expansion of large x . In the reduced velocity expansion, magnetic fields first enter in the x^{-3} term. In the reduced density expansion, magnetic fields first enter in the x^{-6} term. So the MHD solution behaviours at large x are only slightly modified by the presence of magnetic field. The

magnitude of transverse magnetic field B_{\perp} at large distances scales as

$$B_{\perp}^2 = \frac{\lambda a^4 A^2}{Gr^2}.$$

We may get back to nonlinear ODEs (24) and (25) to qualitatively see the leading expansion behaviours of the solutions (60) and (61). In the limit of $x \rightarrow +\infty$, the leading term of v is the constant speed parameter V and the leading term of α is Ax^{-2} . By substituting the leading terms into the following expressions for various relevant forces, we obtain the pressure gradient force in the limit of $x \rightarrow +\infty$ as

$$-\alpha' / \alpha = 2/x,$$

the gravitational force in the limit of $x \rightarrow +\infty$ as

$$-\alpha(x-v) = -\frac{A}{x},$$

and the magnetic pressure and tension forces together in the limit of $x \rightarrow +\infty$ as

$$-\lambda(\alpha' x^2 + 2\alpha x) = 0.$$

From these three expressions, we know that the sum of magnetic pressure and tension forces actually does not affect the dynamic behaviour at very large x (i.e., a nearly force-free condition). When $A > 2$, the inward gravitational force overpowers the pressure gradient force. When $A = 2$, the gravitational force is barely balanced by the pressure gradient force. The latter situation is closely pertinent to the EWCS of Shu (1977).

In the limit of $x \rightarrow 0^+$, the asymptotic solutions for the central free-fall collapse is

$$v \rightarrow -2F/x^{1/2} - \frac{3}{4F}x^{1/2} \ln x - 2Lx^{1/2} + \dots, \quad (63)$$

$$\alpha \rightarrow F/x^{3/2} - \frac{3}{8F}x^{-1/2} \ln x - Lx^{-1/2} + \dots, \quad (64)$$

$$\beta = \lambda\alpha^2 x^2 = \frac{\lambda F^2}{x} + \dots, \quad (65)$$

where $F > 0$ and L are two constant parameters. We may take $F = m_0/\sqrt{2}$ with parameter m_0 being a measure for the central mass accretion rate (Lou & Shen 2004). In dimensional form, the transverse magnetic energy density is

$$\frac{B_{\perp}^2}{8\pi} \rightarrow \frac{\lambda a^3 m_0^2}{16\pi Gtr}.$$

The pressure gradient force in the limit of $x \rightarrow 0^+$ is

$$-\frac{\alpha'}{\alpha} = \frac{3}{2x},$$

the gravitational force in the limit of $x \rightarrow 0^+$ is

$$-\alpha(x-v) = -\frac{2F^2}{x^2},$$

and the sum of the magnetic pressure and tension forces together in the limit of $x \rightarrow 0^+$ is

$$-\lambda(\alpha' x^2 + 2\alpha x) = -\frac{\lambda F}{2x^{1/2}}.$$

In the limit of $x \rightarrow 0^+$, the most dominant force is the gravitational force leading to a gravitational core collapse. The pressure gradient force is the second dominant one. In

comparison, the sum of the magnetic pressure and tension forces is inward and has the weakest effect as $x \rightarrow 0^+$.

The other asymptotic solution for a core expansion as $x \rightarrow 0^+$ is given by

$$v \rightarrow \frac{2}{3}x + \frac{(2 - 3D - 18D\lambda)}{135}x^3 + \dots, \quad (66)$$

$$\alpha \rightarrow D + \frac{D(2 - 3D - 18D\lambda)}{18}x^2 + \dots, \quad (67)$$

$$\beta = \lambda\alpha^2 x^2 = \lambda D^2 x^2 + \dots, \quad (68)$$

which is a fairly straightforward MHD generalization of the Larson-Penston type solutions.

The pressure gradient force in the limit of $x \rightarrow 0^+$ is

$$-\frac{\alpha'}{\alpha} = -\frac{(2 - 3D - 18D\lambda)}{9}x,$$

the gravitational force in the limit of $x \rightarrow 0^+$ is

$$-\alpha(x - v) = -\frac{D}{3}x,$$

and the sum of the magnetic pressure and tension forces in the limit of $x \rightarrow 0^+$ is

$$-\lambda(\alpha' x^2 + 2\alpha x) = -2\lambda D x.$$

By comparing the three forces, it is clear that the magnetic field plays an important dynamical role in the core expansion. This involves a radially inward net magnetic force. By setting λ equal to zero, we readily recover the results of Shu et al. (2002). From equation (66), we know that $v > 0$, $v' > 0$ and $(v - x) < 0$. The total time derivative of $u \equiv av(x)$ is nevertheless negative and the magnetic energy density is simply

$$\frac{B_{\perp}^2}{8\pi} = \frac{\lambda D^2 r^2}{8\pi G t^4}.$$

Please note that the straight line $x - v = 0$ is another special demarcation line of importance, especially for the physical requirement of a positive $m(x)$. In the presence of magnetic field, the magnetosonic critical lines become curved in a characteristic manner. In contrast, the sonic critical line in the absence of magnetic field is a straight line $x - v = 1$ in the first and fourth quadrants. When the magnetic field is included, the magnetosonic critical lines become curves in the first and fourth quadrants. In order to go across the magnetosonic critical line smoothly, the primary and secondary directions of the eigensolutions need to be reanalyzed accordingly. The topological characteristics of the saddle and nodal points have also been changed by the inclusion of magnetic field (see Appendix A for details).

4 NUMERICAL SOLUTIONS OF THE NONLINEAR MHD ODES

We derive global solutions in the semi-complete solution space from $x \rightarrow +\infty$ to $x \rightarrow 0^+$. In fact, there exists a one-to-one correspondence between the semi-complete and complete solutions, because of the invariance property for the time reversal symmetry discussed earlier (see figure 6 of Lou & Shen 2004 for examples). We shall solve below the coupled nonlinear MHD ODEs for similarity solutions making use of the magnetosonic critical line analyses and

the asymptotic solution properties presented in § 3. Numerically, we can construct various types of solutions that may or may not cross the magnetosonic critical line. Integrating from $x \rightarrow +\infty$ with three constant parameters λ , V and A specified in asymptotic solutions (60) and (61), we readily obtain those similarity solutions without crossing the magnetosonic critical line.

For global smooth self-similar solutions satisfying critical conditions (29) – (31) along the magnetosonic line, we need to determine the first derivatives of v and α using the L'Hôpital rule. We then integrate leftward (backward) and rightward (forward) from the magnetosonic critical point. Based on the root properties of quadratic equation (35) for eigenvalues of the radial speed gradient v' , we can figure out the nature of the magnetosonic critical points (e.g., Jordan & Smith 1977; Whitworth & Summers 1985). The magnetosonic critical line with $x - v > 0$ covers the first and fourth quadrants. Points along the magnetosonic critical line in the first quadrant [$0 < x < (1 + 2\lambda)^{1/2}$] are saddle points, while points along the magnetosonic critical line in the fourth quadrant [$(1 + 2\lambda)^{1/2} < x < +\infty$] are nodal points (see Appendix A for details). In the first quadrant, type 1 eigensolutions correspond to negative v gradients and type 2 eigensolutions correspond to positive first derivatives of v . In the fourth quadrant, type 1 eigensolutions correspond to lower absolute values of first derivatives of v and type 2 eigensolutions have larger absolute values of first derivatives of v with both v' being positive (see Appendix A). Numerical integrations away from a saddle point tend to be stable. Unstable or neutrally stable integrations may occur when integrating away from a nodal point (Whitworth & Summers 1985; Hunter 1986; Jordan & Smith 1977). In the following we explore numerically various types of solutions that may or may not intersect the magnetosonic critical line.

4.1 Global solutions without crossing the Magnetosonic Critical Line

The MHD generalization of EWCS of Shu (1977) can be obtained by joining two solution segments. One portion for a central MHD free-fall collapse is to the left of $x = (1 + 2\lambda)^{1/2}$ and the other for a magnetostatic quasi-spherical envelope is to the right of $x = (1 + 2\lambda)^{1/2}$. The inner part of MHD EWCS can be obtained by integrating leftward from $x = (1 + 2\lambda)^{1/2}$ with the first derivatives of v and α given by v'_{c1} and α'_{c1} in equations (36) and (37), respectively. Note that first derivatives v'_{c2} and α'_{c2} cannot be used to integrate leftward. The right portion of the MHD EWCS is the special analytical solution (32). In Figure 3, the MHD EWCS solution is plotted in a heavy solid line. This solution can also be obtained by taking the limit of $A \rightarrow 2^+$. Note that the MHD EWCS is tangential to the magnetosonic critical line at the point $x = (1 + 2\lambda)^{1/2}$. At this point, $\alpha = 2x^{-2}$ and thus

$$(a^2 + v_A^2)/a^2 = 1 + \lambda\alpha x^2 = 1 + 2\lambda.$$

In other words, we have $r/(at) = (a^2 + v_A^2)^{1/2}/a$ corresponding to an MHD collapse wave front travelling outward at the magnetosonic speed $(a^2 + v_A^2)^{1/2}$ (i.e., the fast MHD wave speed perpendicular to the local magnetic field).

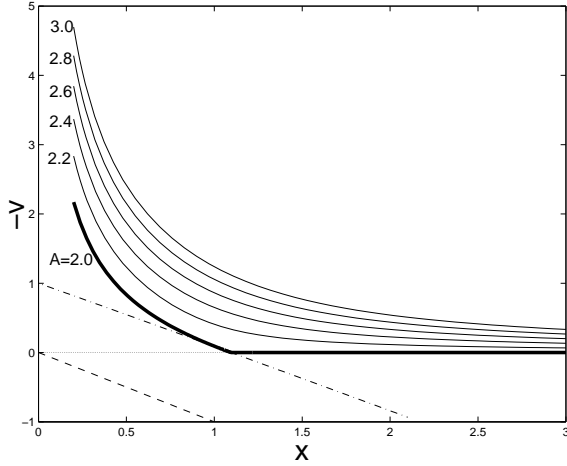


Figure 3. As examples of illustration, we choose $\lambda = 0.1$, $V = 0$, $A = 2.0, 2.2, 2.4, 2.6, 2.8, 3.0$ (from bottom to top in order along the solution curves); the vertical coordinate is $-v$ and the horizontal coordinate is x . This figure is qualitatively similar to figure 1 of Lou & Shen (2004). With a magnetic field included, the critical line has a different shape from that of the pure hydrodynamic case. Dashed line is $x - v = 0$. Dot-dashed line is the curved magnetosonic critical line.

In star forming regions, e.g., the B335 cloud system, a typical mass density in molecular clouds is of the order of 10^{-18} g/cm³ and a typical magnetic field strength is around $100\mu\text{G}$. The Alfvén speed v_A is approximately 0.4 km s⁻¹, which is comparable to the typical sound speed a in molecular cloud cores with temperature of a few tens of Kelvin degrees. Therefore the inclusion of a tangled magnetic field would increase the central mass accretion rate by a factor of ~ 3 or so in the scenario of a magnetized EWCS as compared to the purely hydrodynamic EWCS. The overall dynamical timescale of the infalling envelope would be shortened to a few times 10^4 yr.

The reduced mass density $\alpha(x)$ is continuous at the ‘kink’ point for the magnetosonic collapse front. In the case of an MHD generalization of Shu (1977), the central accretion rate changes with the variation of λ . As λ takes higher values, the core accretion rate becomes greater.

As x approaches infinity, solutions should gradually converge to the asymptotic solutions (60) and (61), while as x approaches the origin, global solutions should satisfy solutions (63), (64), (66) and (67). Those solutions without crossing the magnetosonic critical line can be readily obtained by numerically integrating from the asymptotic solutions (60) and (61) at a sufficiently large x . For those solutions crossing the magnetosonic critical line analytically, the information about the magnetosonic critical line and the gradients of v and α at the critical point is crucial for constructing the solutions.

In Figures 3 – 5, we integrate the coupled nonlinear ODEs (24) and (25) from a large enough x with V , A and λ specified and show global solutions without crossing the magnetosonic critical line. In Figure 3, we numerically integrate the equations with $V = 0$ (the so-called asymptotic breeze solutions; Shen & Lou 2004). For $V < 0$ and $V > 0$ corresponding to inflows and outflows at $x \rightarrow +\infty$ respectively, self-similar solutions can be readily constructed. For

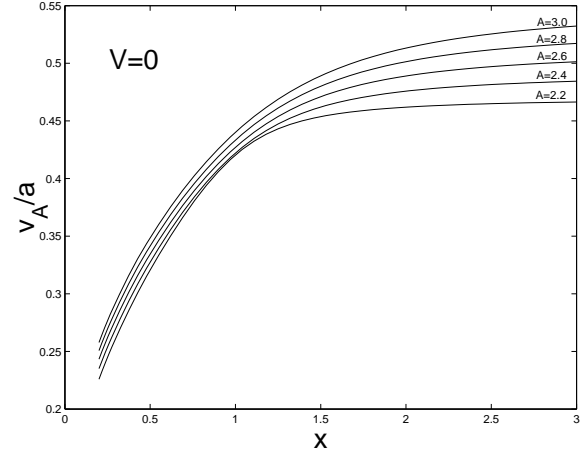


Figure 4. We adopt $\lambda = 0.1$ as in Figure 3. The corresponding Alfvén-to-sound speed ratios v_A/a of similarity solutions with $V = 0$, $A = 2.0, 2.2, 2.4, 2.6, 2.8, 3.0$ (from bottom to top) are displayed; the vertical coordinate is the speed ratio v_A/a and the horizontal coordinate is x .

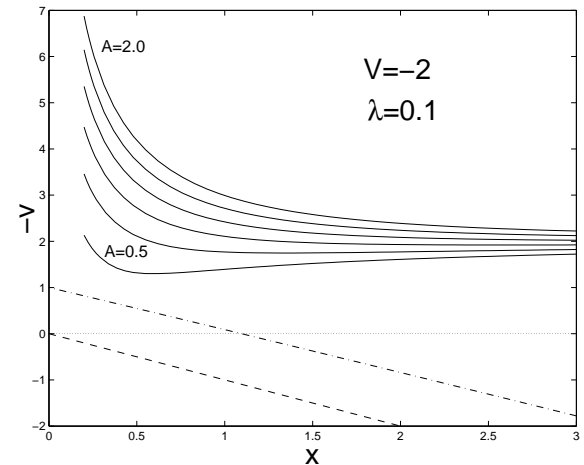


Figure 5. Examples of radial inflows at large x with $\lambda = 0.1$, $V = -2$, $A = 0.5, 0.8, 1.1, 1.4, 1.7, 2.0$, respectively (from bottom to top); the vertical coordinate is $-v$ and the horizontal coordinate is x . The straight dashed line is $x - v = 0$. Dot-dashed line is the magnetosonic critical line.

a specified value of speed parameter V , the mass parameter A should meet certain criteria in order to have global solutions. Due to the nonlinearity of these ODEs and in the presence of magnetic field, this problem is fairly complex and solutions are explored through trial and error (Lou & Shen 2004).

We now summarize some results of our numerical exploration. For numerical solutions with $V = 0$, condition $A > 2$ is necessary for self-similar solutions to exist without crossing the magnetosonic critical line in the first quadrant. For $V < 0$, the lower limit of A for possible similarity solutions without crossing the magnetosonic critical line is less than 2. In our illustrating examples with $\lambda = 0.1$, the lower limit of A is ~ 0.39 . For $A \lesssim 0.39$, similarity MHD solutions would crash onto the magnetocritical line. For $V > 0$ and $\lambda = 0.1$, the minimum value of A for similarity MHD so-

λ	0	0.1	1.0	2.0
m_0	0.98	1.04	1.42	1.73

Table 1. Central mass accretion rates of MHD expansion-wave collapse solution (marked by the heavy solid line in Fig. 3) matched with an isothermal magnetostatic envelope.

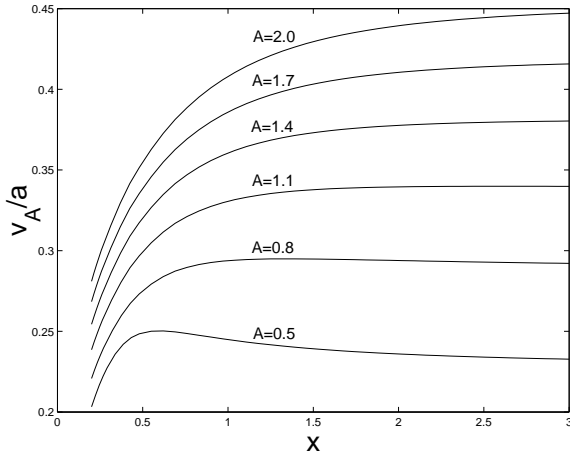


Figure 6. Here $\lambda = 0.1$ as in Figure 5. The corresponding speed ratios of v_A/a for solutions with $V = -2$, $A = 0.5, 0.8, 1.1, 1.4, 1.7, 2.0$ respectively (from bottom to top); the vertical coordinate is the speed ratio v_A/a and the horizontal coordinate is x .

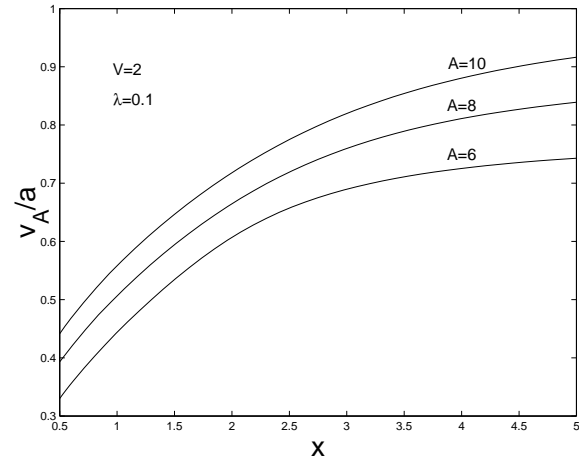


Figure 8. For $\lambda = 0.1$ as in Figure 7, we display the corresponding speed ratios v_A/a for solutions with $V = 2$ and $A = 6, 8, 10$, respectively (from bottom to top); the vertical coordinate is the speed ratio v_A/a and the horizontal coordinate is x .

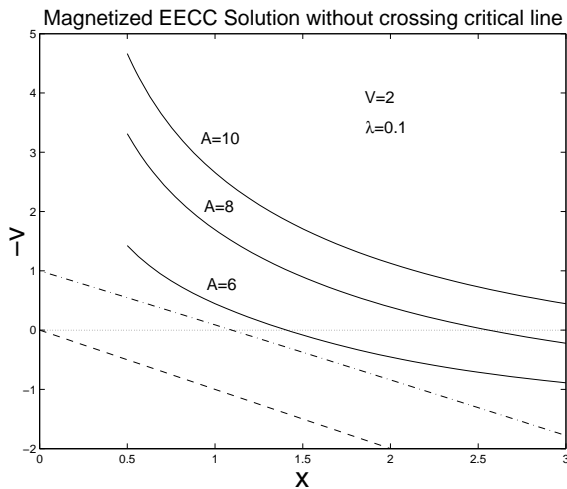


Figure 7. For $\lambda = 0.1$, $V = 2$, and $A = 6, 8, 10$, respectively (from bottom to top), we readily obtain MHD EECC similarity solutions without crossing the magnetosonic critical line; the vertical coordinate is $-v$ and the horizontal coordinate is x . The stagnation point with $-v = 0$ travels outward with a super magnetosonic speed. The straight dashed line is $x - v = 0$. The dash-dotted curve is the magnetosonic critical line.

lutions without crossing the magnetosonic critical line now becomes generally greater than ~ 2 , and varies for different values of V . In our specific computations with $\lambda = 0.1$ and $V = 2$, the minimum value of A is ~ 5.6 . For $A \lesssim 5.6$, the MHD solutions would crash onto the magnetocritical line.

4.2 Analytical Solutions for Crossing the Magnetosonic Critical Line

4.2.1 Type 1 Similarity Solutions

We first describe the type 1 similarity solutions. By integrating leftward and rightward from a point along the magnetosonic critical line with a negative first derivative of $v(x)$, we obtain the type 1 self-similar solutions. These solutions of $v(x)$ in the first quadrant, referred to as the plus solutions by Shu (1977), approach negative constant values of V as $x \rightarrow +\infty$. Following the same procedure, we can also construct type 1 solutions which pass through the magnetosonic critical line in the fourth quadrant. These solutions have the properties that $v(x)$ approaches a positive constant V at large x . We shall see that a class of discrete yet infinitely many type 1 solutions matches finite solutions (66) and (67) near the origin $x = 0$. This type of solutions were first derived by Hunter (1977). Our analysis generalizes these self-similar solutions by including a tangled magnetic field. For further generalizations of LP solutions with various shocks, the interested reader is referred to the recent work of Bian & Lou (2005).

The plus solutions of Shu (1977) (or type 1 solutions, see solution curves in Figure 6) with positive $d(-v)/dx$ in the first quadrant have their counterparts in the presence of magnetic field. They pass through the magnetosonic critical line and approach a constant negative speed V at large x . These solutions may be matched with an approximate quasi-magnetohydrostatic state. As $x \rightarrow 0^+$ and $v \rightarrow 0$, we derive the following equation governing the quasi-magnetohydrostatic state, namely

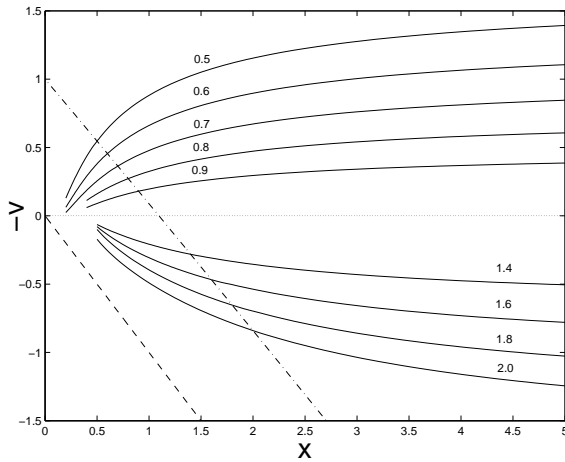


Figure 9. For $\lambda = 0.1$, we show two classes of examples for type 1 solutions smoothly crossing the magnetosonic line in the first and fourth quadrants, separately. The critical points are $x_* = 0.5, 0.6, 0.7, 0.8, 0.9, 1.4, 1.6, 1.8, 2.0$, respectively. The straight dashed line is $x - v = 0$ and the dash-dotted curve is the magnetosonic critical line.

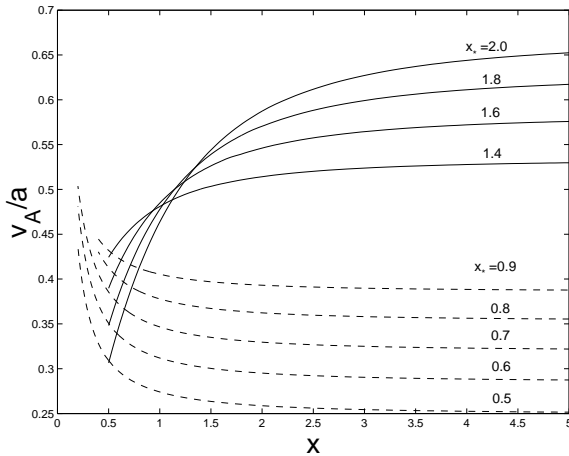


Figure 10. For $\lambda = 0.1$ as in Figure 9, the corresponding Alfvén to sound speed ratios v_A/a of type 1 solutions that smoothly cross the magnetosonic critical line in the first quadrant. The chosen critical points are $x_* = 0.5, 0.6, 0.7, 0.8, 0.9, 1.4, 1.6, 1.8, 2.0$.

$$\frac{1}{x^2} \frac{d}{dx} \left\{ x^2 \left[- (1 + \lambda \alpha x^2) \left(\frac{\alpha'}{\alpha} \right) - 2\lambda \alpha x \right] \right\} = \alpha.$$

For $\lambda = 0$, this equation reduces to the Lane-Emden equation (see relevant discussions in the Appendix of Shu 1977). These solutions represent self-similar inflows with a constant speed at large x . Besides matching with quasi-magnetostatic solutions, it is possible to match these solutions with self-similar outflows at smaller x with or without shocks (Tsai & Hsu 1995; Shu et al. 2002; Shen & Lou 2004; Bian & Lou 2005).

4.2.2 Self-Similar MHD Solutions crossing the Magnetosonic Critical Line Analytically

To find the solutions crossing the magnetosonic critical line analytically, we follow the same procedure of Hunter (1977)

and Lou & Shen (2004). Choosing a meeting point x_m and from different first critical point $x_*(1)$ [$x_*(1) < (1 + 2\lambda)^{1/2}$ and $x_m > x_*(1)$], we integrate the coupled nonlinear MHD ODEs forward towards the meeting point x_m using the type 2 eigensolution. With every $x_*(1)$, we obtain a pair $\{v, \alpha\}$ at the meeting point x_m in the so-called phase diagram of v versus α . For a series of $x_*(1)$, we obtain a series of $\{v, \alpha\}$ pairs and thus a curve in the phase diagram. Similarly, we can integrate the coupled nonlinear MHD ODEs from different $x_*(2)$ [$x_*(2) > (1 + 2\lambda)^{1/2}$ and $x_*(2) > x_m$] backward towards the same meeting point x_m to obtain another curve in the $\{v, \alpha\}$ phase diagram. When we integrate from $x_*(2)$ towards the meeting point x_m , both type 1 and type 2 solutions may be chosen to construct such solutions, while integration from $x_*(1)$ necessarily requires the type 2 solution. Regarding the stability of numerical integrations, we note that to go from $x_*(2)$ towards the meeting point x_m using type 1 solutions, the integration is away from a node along the secondary direction and is neutrally stable. As we go from $x_*(2)$ towards the meeting point x_m using type 2 solutions, the integration is away from a node along the primary direction and is unstable and extremely sensitive to the accuracy of the starting conditions. Based on intersections of the two curves in the $\alpha - v$ phase diagram, we identify matches for global similarity solutions. From these intersection points, we determine the relevant $x_*(1)$ and $x_*(2)$ and compute solutions. Global similarity solutions obtained this way cross the magnetosonic critical line twice analytically.

In Figure 11, we present such a phase diagram of v versus α following the procedure described above. The first three intersection points for $v > -0.5$ in the phase diagram lead to the first three global solutions that cross the magnetosonic critical line twice analytically. For the first solution, we have $0.10306 < x_*(1) < 0.10307$ and $1.81092 < x_*(2) < 1.81093$. For the second solution, we have $0.000128 < x_*(1) < 0.000129$ and $0.8729 < x_*(2) < 0.8730$. For the third solution, we have $1.2 \times 10^{-6} < x_*(1) < 1.3 \times 10^{-6}$ and $1.165 < x_*(2) < 1.166$.

In Figure 12, we display the first three global solutions that go across the magnetosonic critical line twice analytically. Similar oscillation phenomena occur in magnetized cases as those in purely hydrodynamic cases (Lou & Shen 2004). In Figure 13, we present the enlarged part in Figure 12 for small x with a logarithmic scale.

4.2.3 Larson-Penston (LP) Type Solutions and Hunter Type Solutions

Larson (1969a) and Penston (1969a) independently derived a kind of monotonic similarity solution that has the asymptotic behaviour (66) and (67) with $\lambda = 0$ (i.e., without magnetic field) near the origin $x \rightarrow 0^+$. In the presence of magnetic field, the MHD extension of LP solution has the asymptotic behaviour (66) and (67) with $\lambda > 0$. The MHD LP-type solution can be obtained similarly by trying different values of D with a given λ near the origin $x \rightarrow 0^+$ and by integrating nonlinear MHD ODEs (24) and (25) rightward from $x = 0$ towards the magnetosonic critical line $(x - v) + 2\lambda x = (x - v)^3$ until the critical conditions (29)–(31) are satisfied in such a way that the solution matches with one of the two eigensolutions across the magnetosonic critical line. Thus the problem of finding global

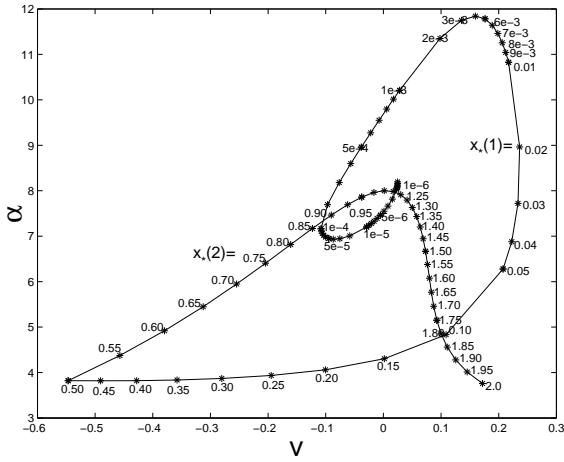


Figure 11. The case of $\lambda = 0.1$. The type 2-type 1 solutions matching phase diagram of v versus α . The meeting point is chosen at $x_m = 0.5$. The type 2 eigenvalue is either positive in the v gradient (saddle point) or of larger absolute value for the v gradient (nodal point). The type 1 is negative in the v gradient (saddle point) or of smaller absolute value for the v gradient (nodal point). The $x_*(1)$ and $x_*(2)$ of the first solution of this type are in the range $0.10306 < x_*(1) < 0.10307$ and $1.81092 < x_*(2) < 1.81093$. For the second solution of this type, we have $0.000128 < x_*(1) < 0.000129$ and $0.8729 < x_*(2) < 0.8730$. As for the third solution of this type, we have $1.2 \times 10^{-6} < x_*(1) < 1.3 \times 10^{-6}$ and $1.165 < x_*(2) < 1.166$.

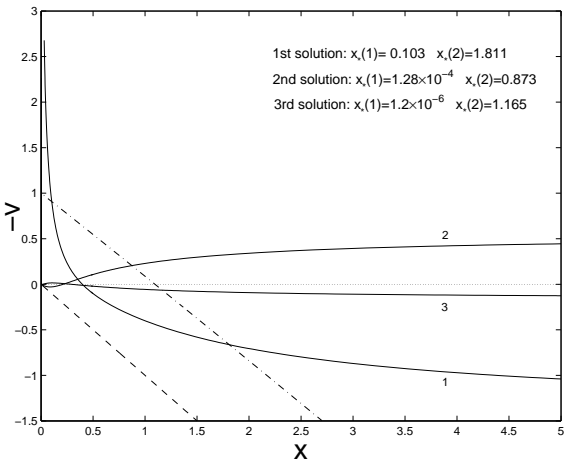


Figure 12. The case of $\lambda = 0.1$. The first three solutions passing across the magnetosonic critical line twice with increasing number of stagnation points moving outward with sub-magnetosonic speeds. We have $x_*(1) \approx 0.10306$ and $x_*(2) \approx 1.81092$ for the first solution with one stagnation point; $x_*(1) \approx 1.28 \times 10^{-4}$ and $x_*(2) \approx 0.873$ for the second solution with two stagnation points; and $x_*(1) \approx 1.2 \times 10^{-6}$ and $x_*(2) \approx 1.165$ for the third solution with three stagnation points. The straight dashed line is $x - v = 0$ and the dash-dotted curve is the magnetosonic critical line.

LP-type solutions is basically an eigenvalue problem of determining discrete eigenvalues for the D parameter.

For the hydrodynamic LP solution, the eigenvalue D is approximately 1.67. In our modified definition of type 1 and type 2 solutions in the presence of magnetic field, the corresponding eigensolutions are related to type 1 solutions

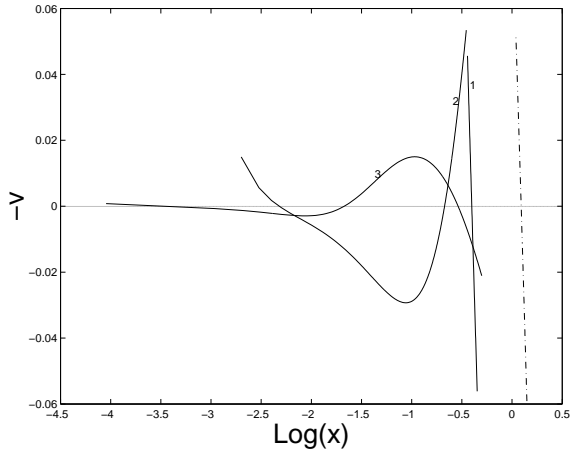


Figure 13. The case of $\lambda = 0.1$. The vertical coordinate is $-v$ and the horizontal coordinate is $\log(x)$. By this enlargement, we see clearly that first the three solutions have one, two, and three stagnation points, respectively. The dash-dotted line is the magnetosonic critical line.

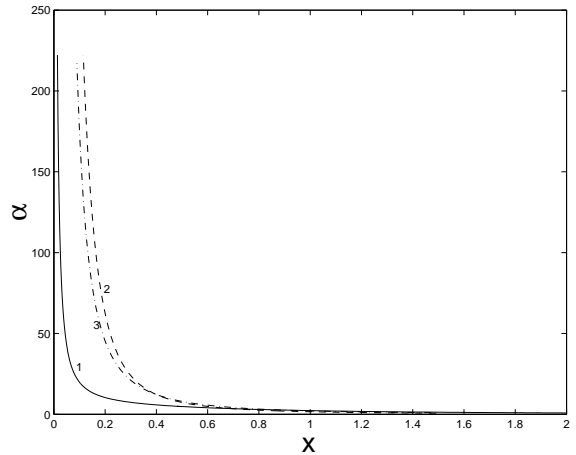


Figure 14. The case of $\lambda = 0.1$. The vertical coordinate is α and the horizontal coordinate is x . The first three solutions go across the magnetosonic critical line analytically. Solid, dashed and dash-dotted curves correspond to the first, second, and third solutions, respectively.

[n.b., not type 2 solutions, see Shu (1977); Hunter (1977); Whitworth & Summers (1985); Lou & Shen (2004)].² LP-type solution goes across the magnetosonic critical line analytically. From our numerical exploration for $\lambda = 0.1$, the corresponding eigenvalue is $D \cong 3.63$. If we relax the constraints that solutions must be analytic (as defined by Hunter 1986) across the magnetosonic critical line, it is then

² In previous studies (Shu 1977; Hunter 1977; Whitworth & Summers 1985; Lou & Shen 2004), while the LP solution is formally classified as type 2 solution (cf. our terminology) across the sonic critical line in the fourth quadrant, the corresponding eigensolution is actually along the secondary direction for $x_* > 2$. Our type 1 and type 2 definitions would not suffer from the disadvantage of magnitude reversal in the sense of dv/dx . By our convention, type 1 is always along the secondary direction, and type 2 is always along the primary direction.

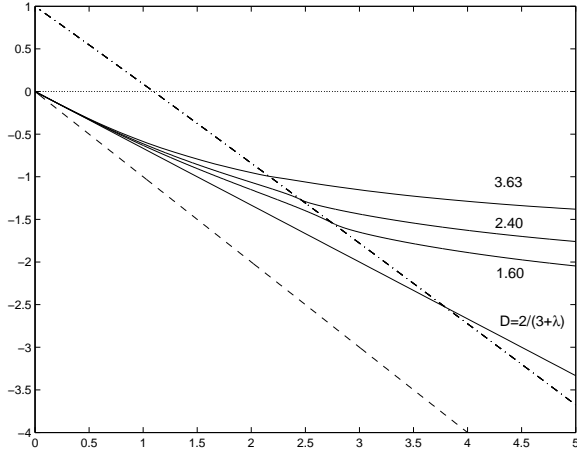


Figure 15. The case of $\lambda = 0.1$. $D = 2/(3+18\lambda)$, 1.60, 2.40, 3.63 running from lower to upper solution curves. LP-type solution passes across the magnetosonic critical line. The straight dashed line is $x - v = 0$. The slightly curved dash-dotted line is the magnetosonic critical line.

possible to construct continuum bands of solutions crossing the magnetosonic critical line with weak discontinuities (Whitworth & Summers 1985). The case of $D = 2/(3+18\lambda)$ corresponds to the special exact global solution (33).

Hunter type solutions refer to those similarity solutions crossing the magnetosonic critical line analytically and having asymptotic behaviour (66) and (67) as x approaches 0. These solutions pass through the magnetosonic critical line along the secondary direction, i.e., they pass the magnetosonic critical line as type 1 solutions. We choose a meeting point at $x_m = 0.5$. From around the origin $x \rightarrow 0^+$ with D and λ specified in equations (66) and (67), we integrate the nonlinear MHD ODEs to the meeting point $x_m = 0.5$. For every D , we obtain a $\{v, \alpha\}$ pair at x_m in the phase diagram. By varying D parameter in sequence, we readily determine a series of $\{v, \alpha\}$ pairs. Plotting this series of $\{v, \alpha\}$, we get a curve in the phase diagram. Meanwhile, we integrate the nonlinear MHD ODEs from different critical points x_* (with $x_* > x_m$) along the magnetosonic critical line backward towards the same meeting point x_m to get another curve in the $\{\alpha, v\}$ phase diagram. Once the intersection points are determined in this phase diagram, we readily obtain the corresponding Hunter type solutions.

5 NOTES AND DISCUSSION

In this paper, we investigated quasi-spherical self-similar flow solutions for magnetized self-gravitating isothermal fluids in the semi-complete solution space. The relevant MHD similarity solutions are obtained and classified by comparing with results of previous analyses (Larson 1969a; Penston 1969a; Shu 1977; Hunter 1977; Whitworth & Summers 1985; Chiueh & Chou 1994; Lou & Shen 2004; Shen & Lou 2004). The straight sonic critical line is now replaced by the curved magnetosonic critical line as expected physically. Global similarity solutions without crossing the magnetosonic critical line also show ECCC and EECC characteristics, and are fairly easy to construct numerically in the isothermal approximation. In a polytropic gas with radiative loss effects,

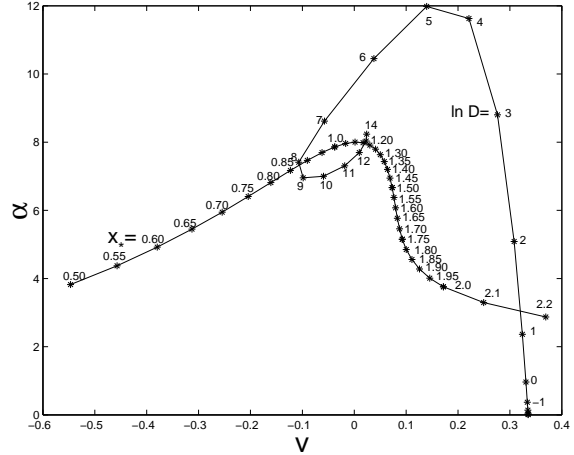


Figure 16. The case of $\lambda = 0.1$. The meeting point is chosen at $x_m = 0.5$. The two parameters D and x_* for the first solution of this type are in the ranges of $1.29 < \ln D < 1.30$ and $2.164 < x_* < 2.165$, respectively. For the second solution of this type, we have $8.15 < \ln D < 8.16$ and $0.8704 < x_* < 0.8705$, respectively. And for the third solution of this type, we have $12.77 < \ln D < 12.78$ and $1.165 < x_* < 1.166$, respectively.

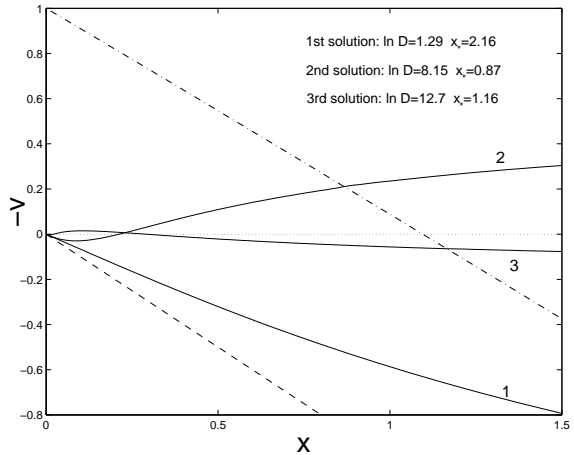


Figure 17. The case of $\lambda = 0.1$ corresponding Fig. 16. The first three Hunter type global solutions across the magnetosonic critical line. The straight dashed line is $x - v = 0$. The dash-dotted curve is the magnetosonic critical line. For the first solution, we have $\ln D = 1.29$ and $x_* = 2.16$; for the second solution, we have $\ln D = 8.15$ and $x_* = 0.87$; and for the third solution, we have $\ln D = 12.7$ and $x_* = 1.16$.

some qualitatively similar features were briefly mentioned in Boily & Lynden-Bell (1995). It is also possible to construct similarity solutions for a magnetized polytropic gas with a quasi-spherical symmetry on larger scales (Wang & Lou 2005, in preparation).

With magnetic field included, both magnetized expansion wave collapse solutions (mEWCS) and magnetized envelope expansion core collapse (mEECC) solutions can be readily constructed. The mEWCS structure is composed of two main parts joined at the collapse wave front $x_* = (1+2\lambda)^{1/2}$. The outer part with $x \geq (1+2\lambda)^{1/2}$ is a nearly force-free magnetostatic envelope with the magnetic pressure and tension forces almost cancelling each other and

the inner part with $x < (1 + 2\lambda)^{1/2}$ is an MHD core collapse characterized by diverging behaviours as $x \rightarrow 0^+$. On the whole, such a mEWCS physically describes a situation with an MHD core collapse approaching a free-fall state in the very central region and with a magnetostatic exterior at rest for $x \geq (1 + 2\lambda)^{1/2}$; the quasi-spherical stagnation surface separating the interior and exterior expands at the magnetosonic speed $(v_A^2 + a^2)^{1/2}$.

For more general mEECC similarity solutions with only one stagnation point x^* along the x -axis, the interior collapse ($x < x^*$) and the exterior expansion ($x \geq x^*$) concur in a self-similar manner. The outward expansion of the exterior envelope gives rise to a wind of constant speed at large radii. The quasi-spherical surface of separation where the gas remains at rest travels outward as time goes on, similar to the ‘expansion-wave front’ of Shu (1977). From a more general perspective, the EWCS of Shu (1977) is a special case of our mEECC similarity solutions in the sense that an unmagnetized outer envelope is static at large x instead of expanding or contracting at constant speeds. The travel speed of the stagnation front at x^* could be either sub-magnetosonic for $x^* < (1 + 2\lambda)^{1/2}$ or super-magnetosonic for $x^* \geq (1 + 2\lambda)^{1/2}$.

This explanation can be straightforwardly extended to those EECC solutions with more than one stagnation points, involving self-similar radial oscillations in sub-magnetosonic region. For such mEECC similarity solutions, there exist more than one quasi-spherical stagnation surfaces of separation that expand outward with time at different constant speeds. The separations between quasi-spherical surfaces increase with time in a self-similar manner.

Such mEECC similarity solutions, which depict an outgoing envelope and a collapsing core, are derived from nonlinear MHD equations and may be applied to various astrophysical processes with proper adaptations. For star-forming regions in molecular clouds, for instance, the starless cloud system B335, we may take an infalling region of spatial scale $\sim 1.5 \times 10^4$ AU, a cloud mass of $\sim 4M_\odot$, a magnetic field strength of $\sim 134 \mu\text{G}$ (Wolf et al. 2003) and a thermal sound speed $a \sim 0.23 \text{ km s}^{-1}$. In this case, the parameter λ is approximately 0.01. By applying the EECC solution that crosses the magnetosonic critical line twice analytically with one stagnation point to model B335 system, we have the following estimates. As cloud materials collapse from a radial distance 7700 AU to 2200 AU in our frozen-in scenario, the magnetic field strength at 2200 AU would become $\sim 300 \mu\text{G}$ and the inflow speed at 2200 AU is $\sim 0.11 \text{ km s}^{-1}$. This inward increase of ‘primordial magnetic field’ may serve as an important ‘seed magnetic field’ for a further enhancement through MHD dynamo processes within the central core of a protostar; the eventual appearance of generic bipolar outflows which are most likely magnetized may result from rotation and symmetry breaking of gross magnetic field configurations. For central collapse regions very much closer to the protostar, our self-similar solutions are not expected to be applicable as transients and feedbacks lead to complicated situations.

Such mEECC similarity solutions with embedded magnetic fields may also be applied to the asymptotic giant branch (AGB) phase or post-AGB phase in the late evolution stage of a star before the gradual emergence evolution of a planetary nebula system with a central white dwarf of a high temperature. The timescale of this evolution ‘gap’ is

estimated to be $\sim 10^3$ yrs. By the conventional wisdom, a main sequence star with a progenitor of less than several solar masses swells tremendously in size and sustains a massive wind with an asymptotic speed of $\sim 10\text{--}20 \text{ km s}^{-1}$; the mass loss rates fall within the range of $\sim 10^{-8}$ to $\sim 10^{-4} M_\odot \text{ yr}^{-1}$. With an insufficient nuclear fuel supply from a certain epoch on, the central region starts to collapse while the outer envelope continues to expand; it is highly likely that the central collapse is accompanied by an outward energetic surge to chase the slowly expanding envelope. Simultaneously, the outer expansion removes stellar envelope mass, while the central infall and collapse produce a proto white dwarf at the center. Sufficiently far away from the initial and boundary conditions, the system may gradually evolve into a dynamic phase representable by an EECC similarity solution during a timescale of a few hundred to several thousand years. Within this rough range of timescale, the accumulation of central core mass should not exceed the Chandrasekhar mass limit of $1.4M_\odot$ for a remnant white dwarf to survive; otherwise, a central explosion (e.g., novae or even a supernova) may occur within a planetary nebula. As a result of the energetic surge, the outer envelope expansion during the EECC phase may be faster than the pre-existing massive slow wind. This process will generally give rise to the formation of outward moving shock when a faster EECC outflow catches up with a slower pre-existing wind. Theoretically, it is possible to construct EECC similarity shock solutions (Shen & Lou 2004; Bian & Lou 2005) to generalize the earlier models of Tsai & Hsu (1995) and Shu et al. (2002). We therefore hypothesize that dynamical evolution of an mEECC phase of around or less than a few thousand years may be the missing linkage between the AGB or post-AGB phase and the gradual appearance of a planetary nebula. Depending on physical parameters of the progenitor star, it might well happen that the core collapse and subsequent central infalls during an mEECC phase lead to an eventual core mass exceeding the Chandrasekhar mass limit of $1.4M_\odot$ and thus induce an explosion with an intensity determined by the actual rate of central mass accretion.

For gross estimates, observations indicate a magnetic field strength of $\sim 1\text{G}$ near the stellar surface at $r \sim 1\text{AU}$ during the AGB phase, decreasing to $\sim 10^{-3}\text{G}$ at $r \sim 10^3\text{AU}$. In the self-similar expansion regime of our model analysis, we have the transverse magnetic field $B_\perp \propto r^{-1}$ (e.g., Lou 1993, 1994), consistent with the measured magnetic field variations observed for AGB stars. Much stronger surface magnetic fields of a white dwarf might be generated and sustained by intrinsic MHD dynamo processes caused by convective differential rotation within the interior of an AGB star (e.g., Blackman et al. 2001).

The transverse magnetic field strength of a mEECC solution in the innermost free-fall collapse region behaves as $B_\perp \propto r^{-1/2}$. For a magnetic field strength of 1G at $r \sim 1\text{AU}$ and the radius of a proto-white dwarf of $\sim 6000 \text{ km}$, the order of magnitude in spatial scale of the system decreases roughly by a factor of $\sim 10^6$ and accordingly the magnetic field strength increases roughly by a factor of $\sim 10^3$. As a result, the magnetic field estimated at the surface of a proto-white dwarf is roughly of the order of $\sim 10^3 \text{ G}$.

For the Crab Nebula as an example of supernova remnant, we simply model the magnetic field as $B_\perp \propto r^{-1}$ during the envelope expansion phase, ignoring complex interac-

tions between the pulsar wind and the inner nebula involved in the expansion of the nebula. For a neutron star with a radius of ~ 10 km and an initial dipolar magnetic field strength of $\sim 10^{10}$ G, the magnetic field would decrease to $\sim 10^{-3}$ G at about several parsecs. These estimates roughly agree with the envelope expansion portion of our simple mEECC solutions.

For astrophysical systems of much larger scales such as clusters of galaxies (e.g., Sarazin 1988; Fabian 1994), the similarity solutions may be valuable for modeling a certain phase of their dynamical evolution involving large-scale random magnetic fields. Specifically, if their evolution involves a self-similar phase of central collapse (Gunn & Gott 1972; Fillmore & Goldreich 1984; Bertschinger 1985; Navarro et al. 1997), then isothermal similarity solutions (63), (64), (66) and (67) seem to suggest two possible classes of galaxy clusters that release X-ray emissions through hot electrons virialized in gravitational potential wells. The bifurcation of extremely high X-ray core luminosities and normal X-ray core luminosities may correspond to steeper and shallower gravitational potential wells, respectively. Typically, a galaxy cluster is characterized by a size of order of a few Mpc, a mass of order of $10^{13} M_{\odot}$, and a magnetic field strength of a few μG .

For a galaxy cluster resulting from a collapse of a gravitationally bound system on much larger scales, a primordial weak magnetic field frozen into the gas can be enhanced by gradual contractions. In the central core collapse region, a transverse magnetic field may scale as $B \propto r^{-1/2}$. In this scenario, specific values of primordial magnetic fields would be determined by the spatial scale when the system starts a self-similar collapse.

While our mEECC and mECCC models are highly simplified and idealized, it would presumably grasp a few fundamental aspects of certain physical processes and provide valuable physical insights into the magnetic field evolution in various astrophysical systems.

ACKNOWLEDGMENTS

This research has been supported in part by the ASCI Center for Astrophysical Thermonuclear Flashes at the University of Chicago under the Department of Energy contract B341495, by the Special Funds for Major State Basic Science Research Projects of China, by the Tsinghua Center for Astrophysics, by the Collaborative Research Fund from the National Science Foundation of China (NSFC) for Young Outstanding Overseas Chinese Scholars (NSFC 10028306) at the National Astronomical Observatories, Chinese Academy of Sciences, by the NSFC grant 10373009 at the Tsinghua University, and by the Yangtze Endowment from the Ministry of Education at the Tsinghua University. The hospitalities of the Mullard Space Science Laboratory at University College London and of Centre de Physique des Particules de Marseille (CPPM/CNRS) + Université de la Méditerranée are also gratefully acknowledged. Affiliated institutions of YQL share this contribution.

REFERENCES

- Adams F. C., Lada C. J., Shu F. H., 1987, *ApJ*, 321, 788
 Balick B., Frank A., 2002, *ARA&A*, 40, 439
 Bertschinger E., 1985, *ApJS*, 58, 39
 Bian F.-Y., Lou Y.-Q., 2005, *MNRAS*, submitted
 Blackman E. G., Frank A., Markiel J. A., Thomas J. H., Van Horn H. M., 2001, *Nature*, 409, 485
 Bodenheimer P., Sweigart A., 1968, 152, 515
 Bondi H., 1952, *MNRAS*, 112, 195
 Boily C. M., Lynden-Bell D., 1995, *MNRAS*, 276, 133
 Bonnor W. B., 1956, *MNRAS*, 116, 351
 Bouquet S., Feix M. R., Fijalkow E., Munier A., 1985, *ApJ*, 293, 494
 Cai M. J., Shu, F. H., 2005, *ApJ*, 618, 438
 Chandrasekhar S., 1957, *Stellar Structure*. Dover Publications, New York
 Cheng A. F., 1978, *ApJ*, 221, 320
 Chiueh T. H., Chou J. K., 1994, *ApJ*, 431, 380
 Choi M., Evans N. J., II, Gregersen E. M., Wang Y., 1995, *ApJ*, 448, 742
 Contopoulos I., Ciolek G. E., Königl A., 1998, *ApJ*, 504, 247
 Ebert R., *Zs. Ap.*, 37, 217
 Fabian A. C., 1994, *ARA&A*, 32, 277
 Falgarone E., Pety J., Phillips T. G., 2001, *ApJ*, 555, 178
 Fillmore J. M., Goldreich P., 1984, *ApJ*, 284, 1
 Foster P. N., Chevalier R. A., 1993, *ApJ*, 416, 303
 Goldreich P., Weber S. V., 1980, 238, 991
 Gunn J. E., Gott III J. R., 1972, *ApJ*, 176, 1
 Hanawa T., Nakayama K., 1997, *ApJ*, 484, 238
 Hanawa T., Matsumoto T., 1999, *ApJ*, 521, 703
 Hanawa T., Matsumoto T., 2000, *PASJ*, 52, 241
 Harada T., Maeda H., Semelin B., 2003, *Phys. Rev. D*, 67, 084003
 Hartmann L., 1998, *Accretion Processes in Star Formation*, Cambridge University Press
 Harvey D. W., Wilner D. J., Myers P. C., Alves J. F., Chen H., 2001, *ApJ*, 563, 903
 Hayashi C., 1966, *ARA&A*, 4, 171
 Hennebelle P., 2003, *A&A*, 397, 381
 Hunter C., 1977, *ApJ*, 218, 834
 Hunter C., 1986, *MNRAS*, 223, 391
 Inutsuka S., Miyama S. M., 1992, *ApJ*, 388, 392
 Jordan D. W., Smith P., 1977, *Nonlinear Ordinary Differential Equations*. Oxford Univ. Press, Oxford
 Kawachi T., Hanawa T., 1998, *PASJ*, 50, 577
 Klessen R. S., Burkert A., 2000, *ApJS*, 128, 287
 Krasnopolsky R., Königl A., 2002, *ApJ*, 580, 987
 Kwok S., 1982, *ApJ*, 258, 280
 Kwok S., 1985, *AJ*, 90, 49
 Kwok S., 1993, *ARA&A*, 31, 63
 Lai D., 2000, *ApJ*, 540, 946
 Lai D., Goldreich P., 2000, *ApJ*, 535, 402
 Landau L. D., Lifshitz E. M., 1959, *Fluid Mechanics* (New York: Pergamon)
 Larson R. B., 1969a, *MNRAS*, 145, 271
 Larson R. B., 1969b, *MNRAS*, 145, 405
 Lou Y. Q., 1993, *ApJ*, 414, 656
 Lou Y. Q., 1994, *ApJ*, 428, L21
 Lou Y. Q., Shen Y., 2004, *MNRAS*, 348, 717
 Maeda H., Harada T., Iguchi H., Okuyama N., 2002,

Progress of Theoretical Physics, 108, 819
McLaughlin D. E., Pudritz R. E., 1997, ApJ, 476, 750
Murakami M., Nishihara K., Hanawa T., 2004, ApJ, 607, 879
Navarro J. F., Frenk C. S., White S. D. M., 1997, ApJ, 490, 493
Ori A., Piran T., 1988, MNRAS, 234, 821
Ostriker E. C., Stone J. M., Gammie C. F., 2001, ApJ, 546, 980
Parker E. N., 1963, Interplanetary Dynamical Processes (New York: Wiley)
Penston M. V., 1969a, MNRAS, 144, 425
Penston M. V., 1969b, MNRAS, 145, 457
Porter D. H., Pouquet A., Woodward P. R., 1994, Phys. Fluid, 6, 2133
Press W. H., Flannery B. P., Teukolsky S. A., Vetterling W., 1986, Numerical Recipes (Cambridge: Cambridge Univ. Press)
Sarazin C. L., 1988, X-Ray Emission from Clusters of Galaxies. Cambridge University Press, Cambridge
Saito M., Sunada K., Kawabe R., Kitamura Y., Hirano N., 1999, ApJ, 518, 334
Scalo J., Vazquez-Semadeni E., Chappell D., Passot T., 1998, ApJ, 504, 835
Sedov L. I., 1959, Similarity and Dimensional Methods in Mechanics (New York: Academic)
Semelin B., Sanchez N., de Vega H. J., 2001, Phys. Rev. D, 63, 4005
Shadmehri M., 2005, 356, 1429
Shen Y., Lou Y. Q., 2004, ApJL, 611, 117
Shu F. H., 1977, ApJ, 214, 488
Shu F. H., Adams F. C., Lizano S., 1987, ARA&A, 25, 23
Shu F. H., Lizano S., Galli D., Cantó J., Laughlin G., 2002, ApJ, 580, 969
Spitzer L., Physical Processes in the Interstellar Medium. Wiley, New York
Suto Y., Silk J., 1988, ApJ, 326, 527
Tanaka T., Washimi H., 2002, Science, 296, 321
Terebey S., Shu F. H., Cassen P., 1984, ApJ, 286, 529
Tilley D. A., Pudritz R. E., 2003, ApJ, 593, 426
Tsai J. C., Hsu J. J. L., 1995, ApJ, 448, 774
Whitworth A., Summers D., 1985, MNRAS, 214, 1
Wolf S., Launhardt R., Henning T., 2003, ApJ, 592, 233
Yahil A., 1983, ApJ, 265, 1047
Zhou S., Evans N. J., II, Kömpe C., Walmsley C. M., 1993, ApJ, 404, 232

APPENDIX A: ANALYSIS OF SADDLE POINTS AND NODAL POINTS

This appendix A is to show explicitly which portion of the magnetosonic critical line corresponds to saddle points and which portion of the magnetosonic critical line corresponds to nodal points (e.g., Jordan & Smith 1977). We examine equation (35) in order to extract information about the signs of the roots of equation (35) along the magnetosonic critical line. In the hydrodynamical case, the roots of equation (35) can be expressed in fairly simple analytical forms. We know that a point within the open interval $0 < x < 1$ along the magnetosonic critical line is a saddle point, while a point

within $x > 1$ along the magnetosonic critical line is a nodal point.

In the presence of magnetic field, saddle and nodal points along the magnetosonic critical line are not so obvious as for the cases without magnetic field. Here, we perform such an analysis. Following the procedure of Whitworth & Summers (1985), we cast the self-similar non-linear MHD ODEs in the forms of

$$dv/dx = Y(x, v, \alpha)/X(x, v, \alpha), \quad (\text{A1})$$

$$d\alpha/dx = Z(x, v, \alpha)/X(x, v, \alpha), \quad (\text{A2})$$

where functionals X , Y , and Z are defined by

$$X(x, v, \alpha) \equiv (x - v)^2 - (1 + \lambda\alpha x^2), \quad (\text{A3})$$

$$Y(x, v, \alpha) \equiv \alpha(x - v)^2 - 2(x - v)/x, \quad (\text{A4})$$

$$Z(x, v, \alpha) \equiv \alpha^2(x - v) + 2\lambda\alpha x^2 - 2\alpha(x - v)^2/x. \quad (\text{A5})$$

We figure out local topological properties of the solutions by examining the eigenvalues of the following matrix

$$M = \begin{pmatrix} \partial X/\partial x & \partial X/\partial v & \partial X/\partial \alpha \\ \partial Y/\partial x & \partial Y/\partial v & \partial Y/\partial \alpha \\ \partial Z/\partial x & \partial Z/\partial v & \partial Z/\partial \alpha \end{pmatrix}$$

with the partial derivatives of X , Y and Z evaluated at a given point along the magnetosonic critical line. Detailed calculations show that one of the three eigenvalues is zero and the other two eigenvalues satisfy the following quadratic equation

$$az^2 + bz + c = 0, \quad (\text{A6})$$

where $a \equiv 1$, $b \equiv -2\zeta$, $c \equiv 2(\zeta - x)(1 - 3\zeta^2)/(\zeta x^2)$ and $\zeta \equiv x - v$ with $\zeta > 0$ and $x > 0$ under consideration. If the two roots of equation (A6) are of the same sign corresponding to the magnetosonic critical point being a nodal point, the requirement is simply $c/a > 0$, or equivalently $ac > 0$; this translates to $(1 - 3\zeta^2)(\zeta - x) > 0$. For $x < \sqrt{3}/3$, we then have

$$0 < -v < \sqrt{3}/3 - x.$$

From Figure (A1) of the magnetosonic critical line, we see that this inequality cannot be realized. On the other hand for $x > \sqrt{3}/3$, it follows that

$$\sqrt{3}/3 - x < -v < 0.$$

Points along the magnetosonic critical line in the range of $x > \sqrt{3}/3$ which also satisfy the above inequality simultaneously must be in the range of $(1 + 2\lambda)^{1/2} < x < +\infty$.

For the case of two real roots, the discriminant must be non-negative. The proof is as follows. In the open interval of $(1 + 2\lambda)^{1/2} < x < +\infty$, we have the inequality $\zeta > (1 + 2\lambda)^{1/2} > 1$ and the discriminant is simply

$$\begin{aligned} b^2 - 4ac &= 4\zeta^2 - 8 \frac{(\zeta - x)(1 - 3\zeta^2)}{x^2\zeta} \\ &= \frac{4x^2\zeta^3 - 8(\zeta - x)(1 - 3\zeta^2)}{x^2\zeta}. \end{aligned} \quad (\text{A7})$$

For a positive denominator, we only need to examine the sign of the numerator

$$\begin{aligned} &4x^2\zeta^3 - 8(\zeta - x)(1 - 3\zeta^2) \\ &= 4\zeta^3 x^2 + (8 - 24\zeta^2)x - (8 - 24\zeta^2)\zeta. \end{aligned}$$

This quadratic expression in terms of x approaches the minimum value of

$$4(-1 + 6\zeta^2 - 11\zeta^4 + 6\zeta^6)/\zeta^3$$

as x takes on the value of $x = (3\zeta^2 - 1)/\zeta^3$, where the numerator can be further factorized into

$$4(3\zeta^2 - 1)(2\zeta^2 - 1)(\zeta + 1)(\zeta - 1).$$

For $\zeta > 1$, this minimum remains always positive and thus the discriminant of the critical quadratic equation remains always positive. We thus come to the conclusion that when the abscissa x of a magnetosonic critical point falls within the open interval $(1 + 2\lambda)^{1/2} < x < +\infty$, it is a nodal point.

In the case of two real roots with opposite signs (i.e., a positive $b^2 - 4ac$ with $ac < 0$) for a magnetosonic critical point being a saddle point, we have $(1 - 3\zeta^2)(\zeta - x) < 0$. When $x < \sqrt{3}/3$, we have either

$$-x < -v < 0 \quad \text{or} \quad \sqrt{3}/3 - x < -v.$$

As seen from Figure (A1), the latter is actually realizable.

On the other hand when $x > \sqrt{3}/3$, we have either

$$-x < -v < \sqrt{3}/3 - x \quad \text{or} \quad 0 < -v.$$

Again from Figure (A1), the latter can be fulfilled along the magnetosonic critical line. Also by Figure (A1), it is clear that the magnetosonic critical line always lies on the upper-right side of the straight line $-v = \sqrt{3}/3 - x$, indicating $-v > \sqrt{3}/3 - x$ along the magnetosonic critical line. Combining these two analyzed cases for saddle type critical points, we come to the conclusion that for $0 < x < (1 + 2\lambda)^{1/2}$ along the magnetosonic critical line, the critical point is of saddle type.

We now summarize the key results of this Appendix A below. Along the magnetosonic critical line, for

$$0 < x < (1 + 2\lambda)^{1/2},$$

the critical point is a saddle point, while for

$$(1 + 2\lambda)^{1/2} < x < +\infty,$$

the critical point is a nodal point.

APPENDIX B: DERIVATION OF THE QUADRATIC EQUATION FOR $V' \equiv Z$

Equation (24) can be rearranged into the form of

$$v' = B/A, \quad (\text{B1})$$

where

$$A \equiv (x - v)^2 - (1 + \lambda\alpha x^2),$$

$$B \equiv (x - v)[\alpha(x - v) - 2/x].$$

Along the magnetosonic critical line, both the denominator A and the numerator B of the above equation vanish. We use the L'Hôpital rule to determine the derivatives at points along the magnetosonic critical line.

The derivative of A with respect x is given by

$$A' = 2(x - v)(1 - v') - 2\lambda\alpha x - \lambda x^2 \alpha'.$$

From equation (21), it follows that

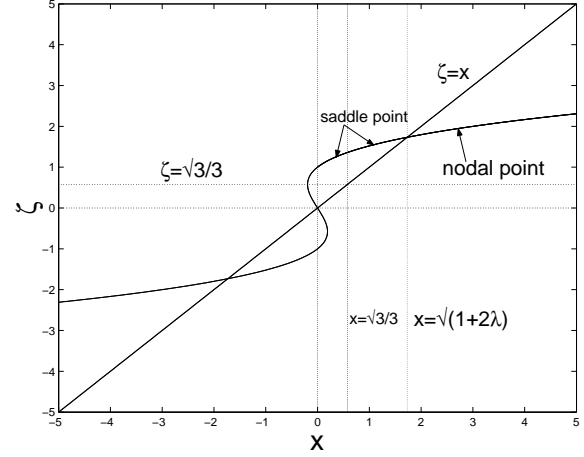


Figure A1. Magnetic field parameter $\lambda = 1$, the vertical coordinate is $\zeta \equiv x - v$, and the horizontal coordinate is $x \equiv r/(at)$. The S shaped curve is the magnetosonic critical line expressed in terms of variable ζ . Combining this figure with our analysis, we can readily distinguish nodal and saddle points along the magnetosonic critical line.

$$\alpha' = \left[\frac{2}{x}(x - v) - v' \right] \frac{\alpha}{(v - x)}.$$

Using this expression in the first derivative of A , we know that A' is a linear expression in terms of $v' \equiv z$, namely

$$A' = f(z),$$

where

$$f(z) \equiv \left[\frac{\lambda\alpha x^2}{(v - x)} - 2(x - v) \right] z + 2(x - v).$$

Meanwhile, we can express the first derivative of B as

$$B' = g(z),$$

where

$$g(z) \equiv -\frac{2v[1 - x(x - v)\alpha]}{x^2} - \frac{x[-2 + x(x - v)\alpha]}{x^2} z.$$

Along the magnetosonic critical line, we have the critical condition that $x(x - v)\alpha = 2$. With this relation, $f(z)$ and $g(z)$ can be reduced to the forms of

$$f(z) = \left[-\frac{2\lambda x}{(x - v)^2} - 2(x - v) \right] z + 2(x - v),$$

$$g(z) = 2v/x^2.$$

By the L'Hôpital rule, we know that $z = g(z)/f(z)$, or equivalently $f(z)z - g(z) = 0$, leading to quadratic equation (35).

Note that when $\lambda = 0$ and thus $x - v = 1$, we recover the results of Shu (1977), namely

$$-2z^2 + 2z - 2(x - 1)/x^2 = 0. \quad (\text{B2})$$

The two roots of this equation are simply

$$z_1 = 1/x_* \quad \text{and} \quad z_2 = 1 - 1/x_*,$$

respectively, where x_* is a point along the sonic critical line. For higher-order expansion terms, see more details of Appendix of Shu (1977) and of Lou & Shen (2004).

APPENDIX C: MAGNETIC PRESSURE AND MAGNETIC TENSION FORCES

In spherical polar coordinates (r, θ, ϕ) , the three r -, θ - and ϕ -components of the magnetic tension force are:

$$(\mathbf{B} \cdot \nabla \mathbf{B})_r = B_r \frac{\partial B_r}{\partial r} + \frac{B_\theta}{r} \frac{\partial B_r}{\partial \theta} + \frac{B_\phi}{r \sin \theta} \frac{\partial B_r}{\partial \phi} - \frac{B_\theta^2 + B_\phi^2}{r}, \quad (\text{C1})$$

$$(\mathbf{B} \cdot \nabla \mathbf{B})_\theta = B_r \frac{\partial B_\theta}{\partial r} + \frac{B_\theta}{r} \frac{\partial B_\theta}{\partial \theta} + \frac{B_\phi}{r \sin \theta} \frac{\partial B_\theta}{\partial \phi} + \frac{B_\theta B_r}{r} - \frac{\cot \theta B_\phi^2}{r}, \quad (\text{C2})$$

$$(\mathbf{B} \cdot \nabla \mathbf{B})_\phi = B_r \frac{\partial B_\phi}{\partial r} + \frac{B_\theta}{r} \frac{\partial B_\phi}{\partial \theta} + \frac{B_\phi}{r \sin \theta} \frac{\partial B_\phi}{\partial \phi} + \frac{B_\phi B_r}{r} + \frac{\cot \theta B_\phi B_\theta}{r}. \quad (\text{C3})$$

Meanwhile, the radial component of the magnetic pressure gradient is

$$\begin{aligned} \left[\frac{1}{2} \nabla(\mathbf{B}^2) \right]_r &= \frac{1}{2} \frac{\partial}{\partial r} (B_r^2 + B_\theta^2 + B_\phi^2) \\ &= B_r \frac{\partial B_r}{\partial r} + \frac{1}{2} \frac{\partial}{\partial r} (B_\theta^2 + B_\phi^2) \\ &= B_r \frac{\partial B_r}{\partial r} + B_\theta \frac{\partial B_\theta}{\partial r} + B_\phi \frac{\partial B_\phi}{\partial r}; \end{aligned} \quad (\text{C4})$$

the θ component of the magnetic pressure gradient is

$$\begin{aligned} \left[\frac{1}{2} \nabla(\mathbf{B}^2) \right]_\theta &= \frac{1}{2r} \frac{\partial}{\partial \theta} (B_r^2 + B_\theta^2 + B_\phi^2) \\ &= \frac{B_r}{r} \frac{\partial B_r}{\partial \theta} + \frac{B_\theta}{r} \frac{\partial B_\theta}{\partial \theta} + \frac{B_\phi}{r} \frac{\partial B_\phi}{\partial \theta}; \end{aligned} \quad (\text{C5})$$

and the ϕ component of the magnetic pressure gradient is

$$\begin{aligned} \left[\frac{1}{2} \nabla(\mathbf{B}^2) \right]_\phi &= \frac{1}{2r \sin \theta} \frac{\partial}{\partial \phi} (B_r^2 + B_\theta^2 + B_\phi^2) \\ &= \frac{B_r}{r \sin \theta} \frac{\partial B_r}{\partial \phi} + \frac{B_\theta}{r \sin \theta} \frac{\partial B_\theta}{\partial \phi} + \frac{B_\phi}{r \sin \theta} \frac{\partial B_\phi}{\partial \phi}. \end{aligned} \quad (\text{C6})$$

Strictly speaking, when the magnetic field is taken into account, a global spherical symmetry cannot be sustained. Checking through equations (C1), (C2), (C3), and equations (C4), (C5), (C6), we see that second and third terms in equation (C1) are ignored. The first term in (C1) and the first term in (C4) cancel each other. In the radial momentum equation, the fourth term in equation (C1) and the second and third terms in equation (C4) are present and kept.

As we take the magnetofluid system to be quasi-spherically symmetric on larger scales, the terms involving $\partial/\partial\theta$ and $\partial/\partial\phi$ are neglected. Thus in the θ and ϕ directions, the first, fourth and fifth terms in equations (C2) and (C3) would cause the overall magnetofluid to be nonspherically symmetric. In order to work in the framework of a quasi-spherical symmetry, we would drop these terms. Nevertheless, we should keep in mind that these terms might give rise to nonspherical shapes of various nebulae in contexts of astrophysics. The quasi-elliptical morphology of the Crab Nebula is a concrete example.